

# Tissue-resident memory CD8<sup>+</sup> T cells promote melanoma-immune equilibrium in skin

Simone L. Park<sup>1</sup>, Anthony Buzzai<sup>2</sup>, Jai Rautela<sup>3,4</sup>, Jyh Liang Hor<sup>1</sup>, Katharina Hochheiser<sup>1,5</sup>, Maike Effer<sup>1,6</sup>, Nathan McBain<sup>1</sup>, Teagan Wagner<sup>2</sup>, Jarem Edwards<sup>7,8,9</sup>, Robyn McConville<sup>1</sup>, James S. Wilmott<sup>8,9</sup>, Richard A. Scolyer<sup>8,9,10</sup>, Thomas Tüting<sup>11</sup>, Umaimainthan Palendira<sup>7,9</sup>, David Gyorki<sup>5,12</sup>, Scott N. Mueller<sup>1,13</sup>, Nicholas D. Huntington<sup>3,4</sup>, Sammy Bedoui<sup>1</sup>, Michael Hölzel<sup>6</sup>, Laura K. Mackay<sup>1,13,14\*</sup>, Jason Waithman<sup>2,14\*</sup> & Thomas Gebhardt<sup>1,14\*</sup>

**The immune system can suppress tumour development both by eliminating malignant cells and by preventing the outgrowth and spread of cancer cells that resist eradication<sup>1</sup>. Clinical and experimental data suggest that the latter mode of control—termed cancer-immune equilibrium<sup>1</sup>—can be maintained for prolonged periods of time, possibly up to several decades<sup>2–4</sup>. Although cancers most frequently originate in epithelial layers, the nature and spatiotemporal dynamics of immune responses that maintain cancer-immune equilibrium in these tissue compartments remain unclear. Here, using a mouse model of transplantable cutaneous melanoma<sup>5</sup>, we show that tissue-resident memory CD8<sup>+</sup> T cells (T<sub>RM</sub> cells) promote a durable melanoma-immune equilibrium that is confined to the epidermal layer of the skin. A proportion of mice (~40%) transplanted with melanoma cells remained free of macroscopic skin lesions long after epicutaneous inoculation, and generation of tumour-specific epidermal CD69<sup>+</sup> CD103<sup>+</sup> T<sub>RM</sub> cells correlated with this spontaneous disease control. By contrast, mice deficient in T<sub>RM</sub> formation were more susceptible to tumour development. Despite being tumour free at the macroscopic level, mice frequently harboured melanoma cells in the epidermal layer of the skin long after inoculation, and intravital imaging revealed that these cells were dynamically surveyed by T<sub>RM</sub> cells. Consistent with their role in melanoma surveillance, tumour-specific T<sub>RM</sub> cells that were generated before melanoma inoculation conferred profound protection from tumour development independently of recirculating T cells. Finally, depletion of T<sub>RM</sub> cells triggered tumour outgrowth in a proportion (~20%) of mice with occult melanomas, demonstrating that T<sub>RM</sub> cells can actively suppress cancer progression. Our results show that T<sub>RM</sub> cells have a fundamental role in the surveillance of subclinical melanomas in the skin by maintaining cancer-immune equilibrium. As such, they provide strong impetus for exploring these cells as targets of future anticancer immunotherapies.**

Most cancers arise within epithelial layers, meaning that immune-cell access to these tissue compartments—including the epidermal layer of the skin—is critical to effective anticancer immunity, particularly at early stages of carcinogenesis. Whereas recirculating T cells (T<sub>CIRC</sub> cells) are largely excluded from the epidermis in the absence of inflammation<sup>6,7</sup>, a distinct population of sessile CD8<sup>+</sup> CD69<sup>+</sup> CD103<sup>+</sup> T<sub>RM</sub> cells populates this anatomical compartment following infection or inflammation<sup>6–9</sup>. Given the important role of T<sub>RM</sub> cells in local and regional immune surveillance<sup>6–11</sup>, we reasoned that they could afford immunity against epidermis-derived skin cancers such as melanoma. This notion

is supported by recent reports indicating a protective function of skin T<sub>RM</sub> cells against intradermally or subcutaneously transplanted tumours<sup>11–14</sup>. However, immunity against epithelial cancers was not addressed in earlier studies and it remained unclear whether T<sub>RM</sub> cells could achieve complete elimination, or whether they mediated long-term suppression of persisting tumour cells.

To investigate these issues, we used a transplantable model of skin-contained tumour development that involves targeting B16 melanoma cells to the outermost layers of mouse skin<sup>5</sup>. We also generated B16 cell variants (B16.gB cells) that express glycoprotein B (gB) from herpes simplex virus (HSV), which allowed us to track transgenic gB-specific CD8<sup>+</sup> T cells (gBT-I cells) responding to melanoma. Contrasting with the rapid tumour development in all mice that follows subcutaneous inoculation of B16.gB cells, epicutaneous transfer to C57BL/6 wild-type mice resulted in delayed tumour formation, with variable growth kinetics and reduced penetrance. In around 60% of mice, epicutaneous inoculation induced tumours that became visible at 2–4 weeks after inoculation, although some developed as late as 6–14 weeks after inoculation (Fig. 1a–c and Extended Data Fig. 1a, b). While most tumours grew progressively, often coinciding with the establishment of metastasis in lymph nodes, others remained small and did not progress for several weeks (Fig. 1c and Extended Data Fig. 1b, c). However, around 40% of mice did not develop melanomas within 4 weeks after inoculation, and were designated ‘non-developers’ if they remained free of macroscopic tumours thereafter (Fig. 1a–c). Spontaneous protection was immune mediated, as mice with genetic defects in various innate and/or adaptive lymphocyte populations—including *Il15*<sup>-/-</sup>, *Rag2*<sup>-/-</sup>; *Il2rg*<sup>-/-</sup> and *Rag1*<sup>-/-</sup> mice—were highly susceptible to melanoma challenge (Fig. 1d–f).

Given that some tumours developed late (Extended Data Fig. 1b), we reasoned that a proportion of non-developers harboured microscopic melanomas long after inoculation. In line with this, we detected B16-derived genomic DNA (gDNA) by droplet digital polymerase chain reaction (ddPCR) in 45 ± 10% of skin samples from non-developers after inoculation with B16.gB.Luc cells, which co-express gB and luciferase (Fig. 1g). In a separate approach, we epicutaneously inoculated B6(Cg)-*Tyr*<sup>-2j</sup> (B6 albino) mice with B16.gB.Luc cells for longitudinal bioluminescence imaging. Macroscopic melanomas emitted strong signals upon luciferin injection, whereas in other mice signals were recorded early after inoculation but then became undetectable over time (Fig. 1h and Extended Data Fig. 1d). Of note, repeated imaging over more than 5 months revealed recurring signals in previously inoculated skin in 9 out of 13 non-developer mice (Fig. 1i–k and Extended Data Fig. 1d).

<sup>1</sup>Department of Microbiology and Immunology, The University of Melbourne at the Peter Doherty Institute for Infection and Immunity, Melbourne, Victoria, Australia. <sup>2</sup>Telethon Kids Institute, University of Western Australia, Perth, Western Australia, Australia. <sup>3</sup>Walter and Eliza Hall Institute for Medical Research, Parkville, Victoria, Australia. <sup>4</sup>Department of Medical Biology, The University of Melbourne, Parkville, Victoria, Australia. <sup>5</sup>Peter MacCallum Cancer Centre, Melbourne, Victoria, Australia. <sup>6</sup>Unit for RNA Biology, Department of Clinical Chemistry and Clinical Pharmacology, University of Bonn, Bonn, Germany. <sup>7</sup>Centenary Institute, The University of Sydney, Sydney, New South Wales, Australia. <sup>8</sup>Melanoma Institute Australia, The University of Sydney, Sydney, New South Wales, Australia. <sup>9</sup>Sydney Medical School, The University of Sydney, Sydney, New South Wales, Australia. <sup>10</sup>Royal Prince Alfred Hospital, Sydney, New South Wales, Australia. <sup>11</sup>Laboratory of Experimental Dermatology, Department of Dermatology, University of Magdeburg, Magdeburg, Germany. <sup>12</sup>Department of Surgery, The University of Melbourne, Parkville, Victoria, Australia. <sup>13</sup>The Australian Research Council Centre of Excellence in Advanced Molecular Imaging, The University of Melbourne, Melbourne, Victoria, Australia. <sup>14</sup>These authors jointly supervised this work: Laura K. Mackay, Jason Waithman, Thomas Gebhardt. \*e-mail: lkmackay@unimelb.edu.au; Jason.Waithman@telethonkids.org.au; gebhardt@unimelb.edu.au

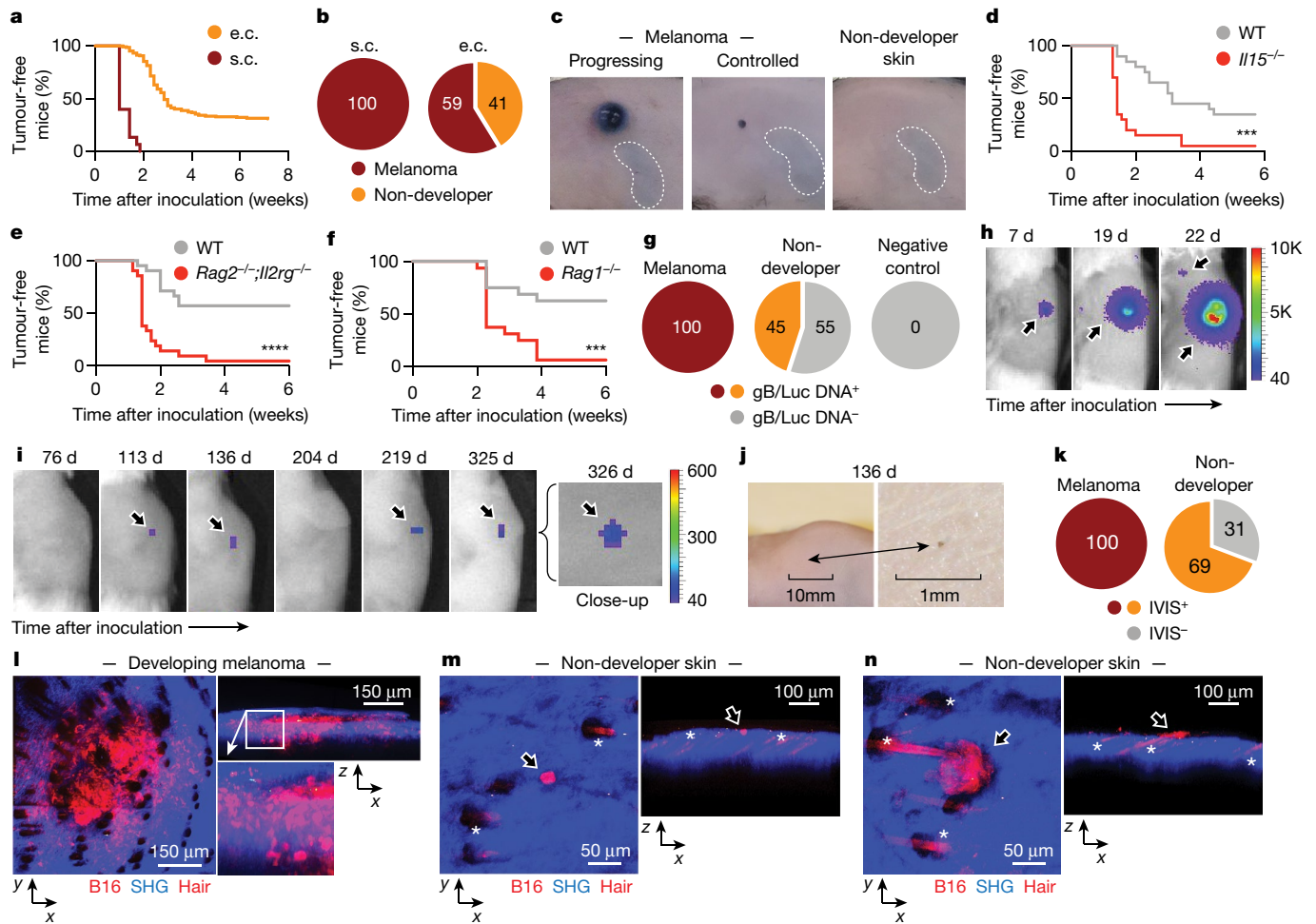


**Fig. 1 | Immune-mediated tumour suppression can result in persistent melanoma.** **a, b**, Proportion of tumour-free (non-developer) and tumour-bearing (melanoma) wild-type mice following epicutaneous (e.c.) or subcutaneous (s.c.) inoculation with B16.gB or B16.gB.Luc cells (pooled analysis). **c**, Disease outcomes 30 days after epicutaneous inoculation. Dotted lines indicate spleen position. Data pooled from  $n = 3$  (s.c.) and  $n = 17$  (e.c.) biologically independent experiments with a total of  $n = 15$  (s.c.) and  $n = 152$  (e.c.) mice (**a**), or pooled from (**b**) or representative of (**c**)  $n = 3$  (s.c.) and  $n = 46$  (e.c.) biologically independent experiments with a total of  $n = 15$  (s.c.) and  $n = 452$  (e.c.) mice. **d–f**, Proportion of tumour-free *Il15*<sup>-/-</sup> (**d**), *Rag2*<sup>-/-</sup>;*Il2rg*<sup>-/-</sup> (**e**) and *Rag1*<sup>-/-</sup> (**f**) mice versus wild-type (WT) mice after e.c. B16.gB inoculation. Data pooled from  $n = 2$  biologically independent experiments with  $n = 20$  (**d**),  $n = 20$  (*Rag2*<sup>-/-</sup>;*Il2rg*<sup>-/-</sup>) or  $n = 21$  (WT) (**e**), or  $n = 16$  (**f**) mice per group. \*\*\* $P = 0.0002$  (**d**) or  $P = 0.0008$  (**f**), \*\*\*\* $P < 0.0001$  (**e**), log-rank Mantel–Cox test. **h**, Detection frequency of gB or Luc gDNA by ddPCR in macroscopic melanoma ( $n = 11$ ), non-developer skin ( $n = 28$ ) or naive skin (negative control;  $n = 8$ ) more than 4 weeks after inoculation

To refine the detection of occult melanomas in non-developer mice, we inoculated B6 albino mice with melanin-pigment-deficient, mCherry-expressing B16.*Tyr*<sup>-/-</sup>.mCherry cells. Subsequent analysis by two-photon microscopy revealed a single-cell-resolution view of melanomas developing in the skin (Fig. 1l and Extended Data Fig. 1e). Notably, two-photon microscopy confirmed the persistence of B16 cells or small clusters in the epidermis of some non-developers (Fig. 1m, n and Extended Data Fig. 1f). Combined, these results suggest that, despite effective immune-mediated tumour suppression, a proportion of disease-free mice failed to achieve complete melanoma eradication from the skin and instead harboured occult B16 cells for long periods of time.

Next we examined the responses of melanoma-specific CD8<sup>+</sup> T cells by tracking congenically marked gBT-I.CD45.1 cells transferred

with B16.gB.Luc cells. Data pooled from  $n = 3$  biologically independent experiments. **h–k**, B6 albino mice were inoculated epicutaneously with B16.gB.Luc cells. **h, i**, Bioluminescence signals detected using an intravital imaging system (IVIS) platform (arrows; different days (d) post-inoculation) in progressing melanoma (**h**) or non-developer skin (**i**). **j**, Miniscule melanoma on mouse in panel **i**. **k**, Proportion of non-developer mice with recurring bioluminescence signals. (IVIS<sup>+</sup> is defined as signal detection in three separate imaging sessions later than 4 weeks post-inoculation.) Data pooled from  $n = 2$  biologically independent experiments incorporating  $n = 13$  non-developers imaged longitudinally for more than five months. **l–n**, Two-photon microscopy images of B16.*Tyr*<sup>-/-</sup>.mCherry cells (red, arrows) in the skin of B6 albino mice with macroscopic melanoma (**l**, 2 weeks post-inoculation) or in non-developer skin (**m, n**; 4 or more weeks post-inoculation). The blue colour shows the second harmonic generation signal (SHG). Note the autofluorescent hair (red, asterisks). Data representative of  $n = 3$  biologically independent experiments with  $n = 22$  mice.

before B16.gB inoculation. Expansion and activation of gBT-I.CD45.1 cells was observed in the skin-draining lymph nodes 7 days after inoculation, and these cells had distributed to spleen and tumour-challenged skin by 2 weeks after inoculation (Extended Data Fig. 2a–g). gBT-I.CD45.1 cells accumulated both within tumours and in peritumoural skin, as well as in the skin of tumour-free non-developer mice (Fig. 2a–d). gBT-I.CD45.1 cells that infiltrated melanomas had a mixed CD69<sup>+/−</sup> phenotype and were CD103<sup>−</sup>, whereas most gBT-I.CD45.1 cells in peritumoural skin were CD69<sup>+</sup> and CD103<sup>+</sup> (Fig. 2a and Extended Data Fig. 2h). Of note, most mice that remained tumour-free 2–4 weeks after inoculation generated CD69<sup>+</sup> CD103<sup>+</sup> gBT-I T<sub>RM</sub> cells in the skin, and such responses were observed more frequently and at higher densities than in the skin of tumour-bearing mice (Fig. 2c, d). T<sub>RM</sub> formation was not dependent on local antigen recognition: OT-I

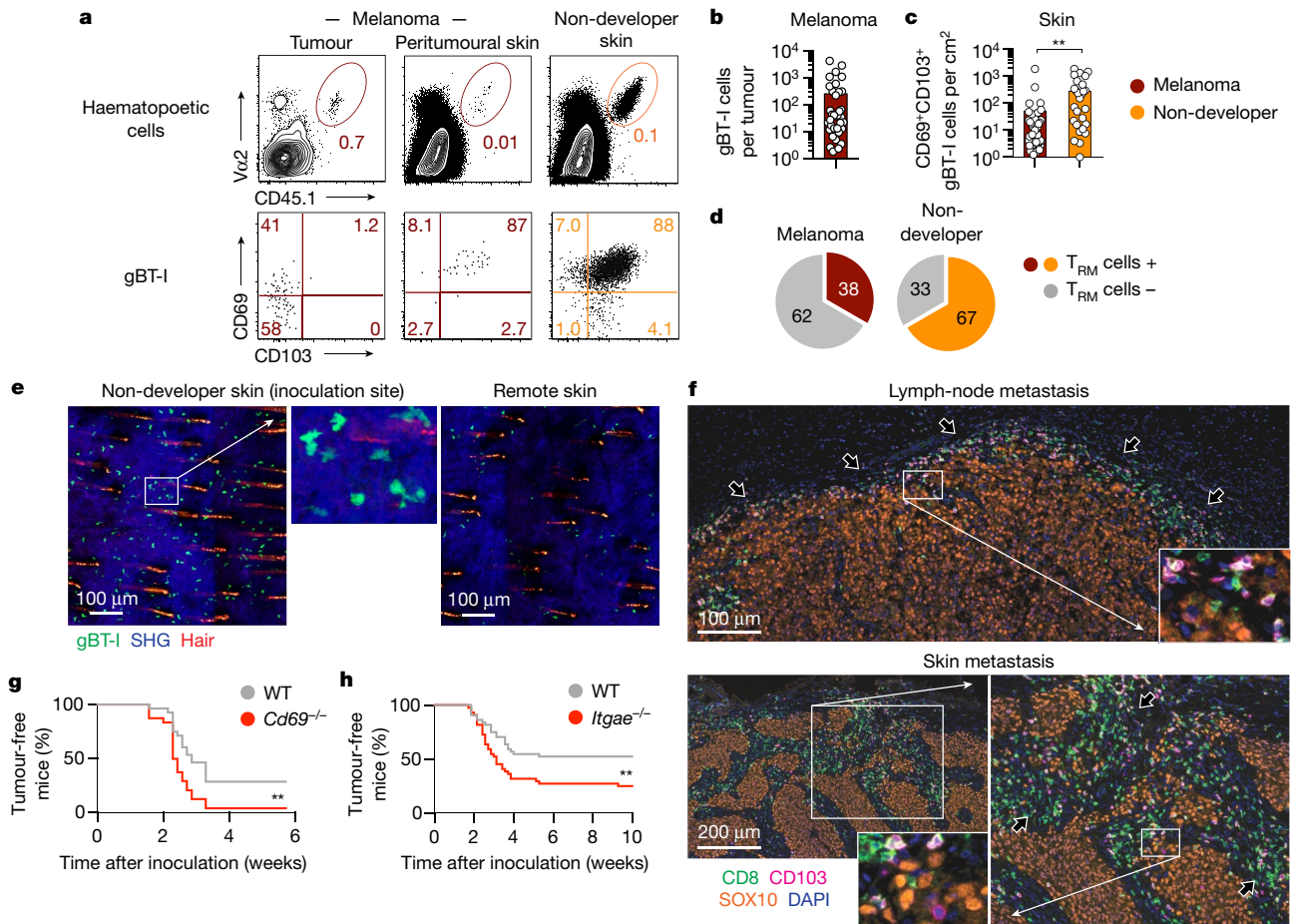


**Fig. 2 | Generation of melanoma-specific  $T_{RM}$  cells in skin.** **a–d**, WT mice received naive gBT-I.CD45.1 cells before e.c. inoculation with B16.gB. Shown are the phenotype (**a**) and numbers (**b**, **c**) of gBT-I.CD45.1 cells infiltrating tumours, peritumoural skin and non-developer skin more than 3 weeks post-inoculation. **d**, Proportion of mice possessing more than 10 gBT-I.CD45.1  $T_{RM}$  cells ( $T_{RM}$  cells +) per  $cm^2$  of peritumoural skin (maroon) or tumour-free skin (orange). Data are representative of (**a**) or pooled from (**b–d**)  $n = 7$  biologically independent experiments with  $n = 50$  (**b**) or  $n = 52$  ('Melanoma') and  $n = 33$  ('Non-developer') mice (**c**).  $**P = 0.0012$ , Mann–Whitney test (**c**). **e**, WT mice received naive gBT-I.uGFP cells before e.c. inoculation with B16.gB.mCherry cells. Two-photon microscopy analysis of the inoculation site (left panel) and remote

(right panel) skin in non-developer mice. gBT-I.uGFP cells are in green and SHG in blue. Note autofluorescent hairs (red/orange). Images are representative of  $n = 2$  biologically independent experiments with  $n = 4$  mice. **f**, Multiplex immunofluorescence microscopy of human lymph-node (upper panel,  $n = 68$ ) and cutaneous (lower panel,  $n = 3$ ) melanoma metastases. Arrows indicate examples of  $CD103^+ CD8^+$  T cells at tumour margins. CD8, green; CD103, pink; SOX10 (melanoma), orange; DAPI, blue. **g**, **h**, Proportion of non-developers amongst  $Cd69^{-/-}$  (**g**),  $Itgae^{-/-}$  (**h**) and WT mice following e.c. B16.gB inoculation. Data pooled from  $n = 3$  (**g**) or  $n = 4$  (**h**) biologically independent experiments with  $n = 44$  mice per group (**h**) or  $n = 28$  (WT) or  $n = 24$  ( $Cd69^{-/-}$ ) mice (**g**).  $**P = 0.0029$  (**g**), 0.0070 (**h**), log-rank Mantel–Cox test.

$CD8^+$  T cells with unrelated specificity and activated by concurrent skin infection with HSV–ovalbumin showed similar upregulation of CD69 and CD103 in peritumoural skin (Extended Data Fig. 3a–d).

We confirmed the accumulation of epidermal  $T_{RM}$  cells in non-developer skin by using intravital two-photon microscopy to track gBT-I cells expressing green fluorescent protein (gBT-I.uGFP) in B16.gB-challenged B6 albino mice (Fig. 2e). Consistent with previous reports<sup>14–17</sup>,  $CD103^+ CD8^+$  T cells were also readily detected in human metastatic melanoma and were frequently concentrated at the margins of tumour nodules (Fig. 2f), reminiscent of their peritumoural localization in mouse skin (Fig. 2a). Increased accumulation of tumour-associated  $CD103^+ CD8^+$  T cells was recently shown to correlate with improved survival in patients with metastatic melanoma<sup>17</sup>. Thus, to test whether efficient generation of  $T_{RM}$  cells was required for melanoma control, we inoculated  $Cd69^{-/-}$  (CD69-deficient) and  $Itgae^{-/-}$  (CD103-deficient) mice, which are known to be impaired in the formation and persistence, respectively, of skin  $T_{RM}$  cells<sup>18</sup>. Both  $Cd69^{-/-}$  and  $Itgae^{-/-}$  mice were more susceptible to melanoma formation than were wild-type mice (Fig. 2g, h). The strong defect in melanoma control in  $Cd69^{-/-}$  mice could be rescued by transfer of naive wild-type gBT-I cells but not gBT-I. $Cd69^{-/-}$  cells before challenge

with B16.gB cells (Extended Data Fig. 4), implying that lack of CD69 expression by  $CD8^+$  T cells and, consequently, impaired  $T_{RM}$  formation<sup>18</sup> led to the inability of  $Cd69^{-/-}$  mice to suppress tumour development. Thus, the accumulation of  $T_{RM}$  cells in skin corresponded with melanoma control, whereas impaired  $T_{RM}$  formation was associated with increased susceptibility. Further supporting the importance of  $CD8^+$  T cells to tumour control, B16.gB cells from small non-progressing melanomas expressed higher levels of major histocompatibility complex I (MHC I) proteins than those in rapidly progressing melanomas (Extended Data Fig. 5).

We predicted that melanoma control required interactions between gBT-I and B16.gB cells. Therefore, we imaged B6 albino mice by intravital two-photon microscopy to track the responses of gBT-I.uGFP cells to inoculation with gB-expressing B16.gB. $Tyr^{-/-}$ .mCherry cells in developer and non-developer mice. We observed varying degrees of gBT-I.uGFP infiltration in or around developing melanomas (Fig. 3a, Extended Data Fig. 6a and Supplementary Video 1). These gBT-I.uGFP cells displayed a spectrum of behaviours while interacting with B16.gB. $Tyr^{-/-}$ .mCherry cells, including prolonged arrest and probing activity, as well as rapid migration (Fig. 3a and Supplementary Video 1). In non-developer skin, most gBT-I cells were epidermal and displayed

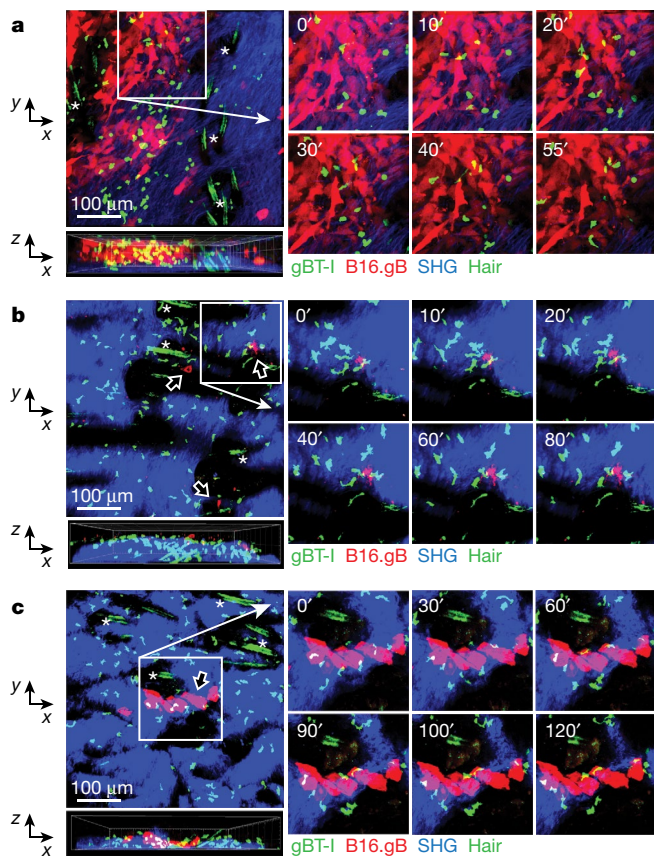


**Fig. 3 | T<sub>RM</sub> cells dynamically survey B16 melanoma in skin.** B6 albino mice received naive gBT-I.uGFP cells before e.c. inoculation with B16.gB.*Tyr*<sup>-/-</sup>.mCherry cells. Shown are two-photon microscopy images and time-lapse series (at the indicated minutes (')) of gBT-I.uGFP cells interacting with B16.gB.*Tyr*<sup>-/-</sup>.mCherry cells in macroscopic melanoma more than 2 weeks post-inoculation (a) or in the skin of non-developers at more than 4 weeks post-inoculation. (b, c). Data are representative of *n* = 3 biologically independent experiments with *n* = 17 mice. B16.gB.*Tyr*<sup>-/-</sup>.mCherry cells (B16.gB; arrows) are in red; gBT-I.uGFP cells (gBT-I) are in green; SHG is in blue. Note the autofluorescent hair (green, asterisks).

crawling behaviour and dendritic protrusions characteristic of T<sub>RM</sub> cells generated by skin infection<sup>6,9</sup> (Fig. 3b, c, Extended Data Fig. 6b and Supplementary Videos 2, 3). Of note, gBT-I.uGFP T<sub>RM</sub> cells colocalized with epidermal B16.gB.*Tyr*<sup>-/-</sup>.mCherry cells that persisted in the absence of macroscopic tumours, and such contacts lasted up to 2 hours (Fig. 3b, c and Supplementary Videos 2, 3). These dynamic interactions were consistent with active immune surveillance and suggested that T<sub>RM</sub> cells were involved in tumour suppression.

To investigate the protective potential of melanoma-specific T<sub>RM</sub> cells, we generated gB-specific T<sub>CIRC</sub> and T<sub>RM</sub> cells by infecting the skin with HSV-1, as described<sup>6,8</sup>. When challenged with B16.gB cells more than 4 weeks later, HSV-immune mice were protected from tumour development (Fig. 4a), although B16-derived gDNA was detected in the skin of almost half of these mice (Extended Data Fig. 7). This protection was antigen specific: HSV-immunized mice failed to suppress tumours after challenge with B16.Ova cells (Fig. 4b). Next, we locally deposited *in vitro* activated gBT-I.CD45.1 cells by epicutaneous transfer, yielding CD103<sup>+</sup> CD69<sup>+</sup> T<sub>RM</sub> cells in the skin together with a small population of T<sub>CIRC</sub> cells that variably egressed from the skin (Extended Data Fig. 8a, b). These mice—but not those with control OT-I T<sub>RM</sub> cells—were protected from B16.gB challenge more than 4 weeks later (Fig. 4c).

To test whether T<sub>RM</sub> cells alone could afford protection, we repeated these experiments with Thy1.1-expressing gBT-I.Thy1.1 cells, which allowed us to selectively deplete T<sub>CIRC</sub> cells by intraperitoneal treatment

with low-dose anti-Thy1.1 antibody, as described<sup>19</sup> (Fig. 4d and Extended Data Fig. 8c, d). The majority of mice suppressed tumour development irrespective of T<sub>CIRC</sub> depletion, even in the absence of endogenous T cells in *Rag1*<sup>-/-</sup> mice, although protection was most pronounced in mice harbouring both T<sub>RM</sub> and T<sub>CIRC</sub> cells (Fig. 4e, f). Finally, we investigated the contribution of T<sub>RM</sub> cells to the control of persistent melanoma cells in non-developer skin. To this end, mice with gBT-I.Thy1.1 T<sub>RM</sub> cells were depleted of T<sub>CIRC</sub> cells and, more than 1 week later, were challenged with B16.gB cells. Non-developers were then depleted of T<sub>RM</sub> cells by intradermal treatment with high-dose anti-Thy1.1 antibody more than 4 weeks later (Fig. 4g and Extended Data Fig. 8e, f). T<sub>RM</sub> depletion triggered melanoma outgrowth in a proportion of previously tumour-free mice (5 out of 29), whereas no skin tumours developed in control mice (0 of 26) (Fig. 4h). The observation that tumour outgrowth was not evident in all mice is probably related to incomplete T<sub>RM</sub> depletion, protection by non-depleted endogenous T<sub>RM</sub> cells, and/or melanoma elimination in some mice before T<sub>RM</sub> depletion. Regardless, the combined results indicate that T<sub>RM</sub> cells can provide tumour surveillance by actively promoting melanoma-immune equilibrium.

To elucidate the potential mechanisms involved in melanoma control, we inoculated wild-type mice alongside mice deficient in the production of the effector molecules perforin, interferon- $\gamma$  (IFN- $\gamma$ ) or tumour-necrosis factor- $\alpha$  (TNF- $\alpha$ ). Perforin-deficient (*Perf1*<sup>-/-</sup>) and IFN- $\gamma$ -deficient (*Ifng*<sup>-/-</sup>) mice had similar tumour incidences to wild-type controls (Extended Data Fig. 9a, b), whereas *Tnfa*<sup>-/-</sup> mice had higher incidences than wild-type controls (Fig. 4i). gBT-I T<sub>RM</sub> cells generated after melanoma challenge could produce IFN- $\gamma$  and TNF- $\alpha$  upon antigen stimulation *in situ*, indicating that they were functional despite expression of immune-checkpoint receptors such as PD-1 (Extended Data Fig. 10a–e). Finally, we generated wild-type or *Tnfa*<sup>-/-</sup> gBT-I T<sub>RM</sub> cells in *Tnfa*<sup>-/-</sup> mice before B16.gB challenge, as in Fig. 4c. TNF- $\alpha$ -deficient gBT-I cells were less efficient at suppressing tumour outgrowth in *Tnfa*<sup>-/-</sup> mice than were wild-type gBT-I cells (Fig. 4j). These results are consistent with previous reports indicating that TNF- $\alpha$  is involved in long-term melanoma control<sup>20</sup>, and that TNF- $\alpha$  together with IFN- $\gamma$  can drive cancer senescence<sup>21</sup>.

Combined, our results provide unequivocal evidence that effective tumour suppression can result in a dynamic melanoma-immune equilibrium in skin and that such lesions can remain clinically occult for prolonged periods of time, if not indefinitely. Although our findings echo clinical and experimental data describing cancer-immune equilibrium as an element of effective cancer surveillance<sup>1–4</sup>, this mode of immunity has remained inherently difficult to study at the cellular level. Critically, we identify T<sub>RM</sub> cells as important drivers of the equilibrium state, in line with previous reports linking the accumulation of these cells with enhanced anticancer immunity in patients<sup>17,22–26</sup> and mouse models<sup>12–14,26</sup>. The densities of T<sub>RM</sub> cells that co-localize with persisting melanoma cells are probably below those required for effective target-cell killing<sup>27,28</sup>, providing one possible explanation as to why melanoma cells are not completely eliminated. This emphasizes the importance of complementary, non-cytolytic mechanisms of control involving cytokines such as TNF- $\alpha$ . Of note, the function of T<sub>RM</sub> cells in controlling persisting melanomas is reminiscent of their presumed role in the local containment of persisting and latent-reactivating viruses, such as HSV and Epstein–Barr Virus<sup>11,29,30</sup>, implying that T<sub>RM</sub>-mediated control of persisting threats via suppression and containment rather than elimination is a broadly operative mode of immunity. In summary, our results provide strong impetus for exploring T<sub>RM</sub> cells as prognostic markers and future targets of cancer immunotherapies.

### Online content

Any methods, additional references, Nature Research reporting summaries, source data, statements of data availability and associated accession codes are available at <https://doi.org/10.1038/s41586-018-0812-9>.

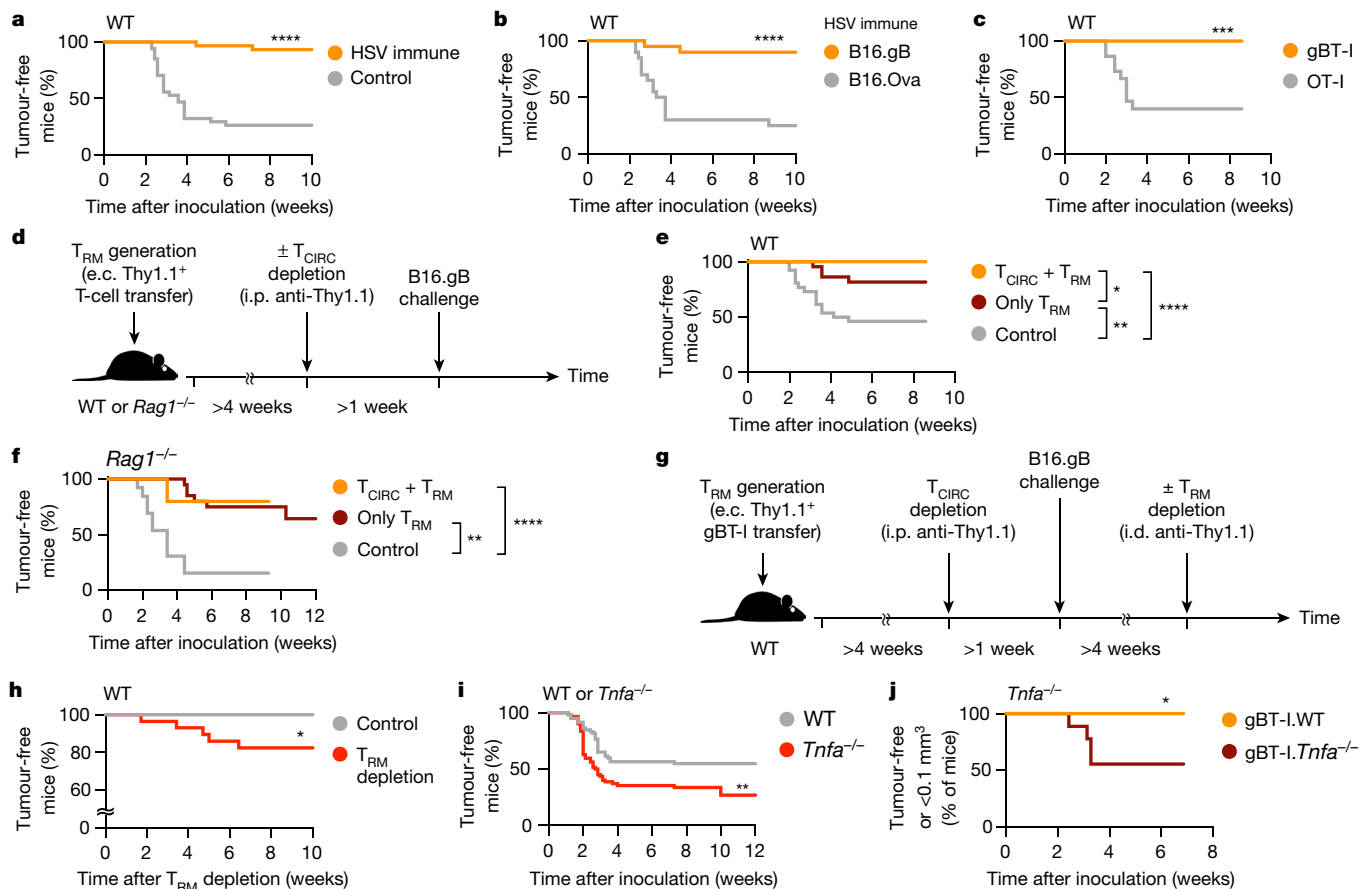


**Fig. 4 | Melanoma-specific  $T_{RM}$  cells promote cancer-immune equilibrium.** **a**, WT mice were infected with HSV on flank skin and challenged with B16.gB cells at more than 4 weeks post-inoculation. The proportion of non-developers among HSV-immune and naive (control) mice is shown. Data pooled from  $n = 4$  biologically independent experiments with  $n = 34$  (control) or  $n = 30$  (HSV immune) mice.  $****P < 0.0001$ . **b**, The same set-up was used as in panel **a**, except that HSV-immune mice were challenged with either B16.gB or B16.Ova cells. Data pooled from  $n = 2$  biologically independent experiments with  $n = 20$  mice per group.  $****P = 0.0001$ . **c**, WT mice were inoculated with e.c. activated gBT-I.CD45.1 (gBT-I) or OT-I.CD45.1 (OT-I) cells and challenged with B16.gB cells at the site of T-cell transfer more than 4 weeks later. Data pooled from  $n = 2$  biologically independent experiments with  $n = 15$  (OT-I) or  $n = 16$  (gBT-I) mice.  $***P = 0.0002$ . **d**, Experimental protocol. WT or  $Rag1^{-/-}$  recipient mice (Thy1.2<sup>+</sup>) were transferred with e.c. activated gBT-I.Thy1.1 (Thy1.1<sup>+</sup>) cells ( $4 \times 10^6$ ) and treated with anti-Thy1.1 antibody more than 4 weeks later. Mice were challenged e.c. with B16.gB or B16.gB.Luc cells later than 1 week post-depletion. **e**, **f**, Proportion of non-developers among WT (**e**) and  $Rag1^{-/-}$  (**f**) mice in anti-Thy1.1-treated (only  $T_{RM}$ ) or PBS-treated ( $T_{CIRC} + T_{RM}$ ) mice

compared with naive mice (control). Data pooled from  $n = 4$  biologically independent experiments with  $n = 22$  (only  $T_{RM}$  and  $T_{CIRC} + T_{RM}$ ) or  $n = 26$  (control) mice (**e**), or  $n = 3$  biologically independent experiments with  $n = 20$  (only  $T_{RM}$ ),  $n = 10$  ( $T_{CIRC} + T_{RM}$ ) or  $n = 13$  (control) mice (**f**).  $*P = 0.0381$ ,  $**P = 0.0074$  (**e**),  $0.0018$  (**f**),  $****P < 0.0001$ . **g**, Experimental protocol. This is the same set-up as in panel **d**, except that non-developers after B16.gB challenge were further treated intradermally (i.d.) with high-dose anti-Thy1.1 antibody at more than 4 weeks post-inoculation to deplete  $T_{RM}$  cells **h**, Proportion of mice remaining tumour-free after  $T_{RM}$  depletion. Data pooled from  $n = 5$  biologically independent experiments with  $n = 29$  ( $T_{RM}$  depletion) or  $n = 26$  (control) mice.  $*P = 0.0286$ . **i**, Proportion of non-developers amongst  $Tnfa^{-/-}$  and WT mice after e.c. B16.gB inoculation. Data pooled from  $n = 6$  biologically independent experiments with  $n = 62$  ( $Tnfa^{-/-}$ ) and  $n = 60$  (WT) mice.  $**P = 0.0042$ . **j**,  $Tnfa^{-/-}$  mice were transferred epicutaneously with gBT-I. WT or gBT-I. $Tnfa^{-/-}$  cells and challenged with B16.gB cells more than 4 weeks later. The proportion of tumour-free mice or mice with tumours that remained less than  $0.1 \text{ mm}^3$  in volume is shown. Data pooled from  $n = 2$  biologically independent experiments with  $n = 9$  ( $Tnfa^{-/-}$ ) or  $n = 10$  (WT) mice.  $*P = 0.0205$ . All statistics by log-rank Mantel-Cox test.

Received: 4 May 2018; Accepted: 1 November 2018;  
Published online: 31 December 2018

- Schreiber, R. D., Old, L. J. & Smyth, M. J. Cancer immunoeediting: integrating immunity's roles in cancer suppression and promotion. *Science* **331**, 1565–1570 (2011).
- Mackie, R. M., Reid, R. & Junor, B. Fatal melanoma transferred in a donated kidney 16 years after melanoma surgery. *N. Engl. J. Med.* **348**, 567–568 (2003).
- Koebel, C. M. et al. Adaptive immunity maintains occult cancer in an equilibrium state. *Nature* **450**, 903–907 (2007).
- Teng, M. W. et al. Opposing roles for IL-23 and IL-12 in maintaining occult cancer in an equilibrium state. *Cancer Res.* **72**, 3987–3996 (2012).
- Wylie, B. et al. Cross-presentation of cutaneous melanoma antigen by migratory  $XCRI^+CD103^-$  and  $XCRI^+CD103^+$  dendritic cells. *Oncolmmunology* **4**, e1019198 (2015).
- Gebhardt, T. et al. Different patterns of peripheral migration by memory  $CD4^+$  and  $CD8^+$  T cells. *Nature* **477**, 216–219 (2011).
- Jiang, X. et al. Skin infection generates non-migratory memory  $CD8^+$   $T_{RM}$  cells providing global skin immunity. *Nature* **483**, 227–231 (2012).
- Gebhardt, T. et al. Memory T cells in nonlymphoid tissue that provide enhanced local immunity during infection with herpes simplex virus. *Nature Immunol.* **10**, 524–530 (2009).
- Ariotti, S. et al. Tissue-resident memory  $CD8^+$  T cells continuously patrol skin epithelia to quickly recognize local antigen. *Proc. Natl Acad. Sci. USA* **109**, 19739–19744 (2012).
- Mackay, L. K. et al. Long-lived epithelial immunity by tissue-resident memory T ( $T_{RM}$ ) cells in the absence of persisting local antigen presentation. *Proc. Natl Acad. Sci. USA* **109**, 7037–7042 (2012).
- Gebhardt, T., Palendira, U., Tschärke, D. C. & Bedoui, S. Tissue-resident memory T cells in tissue homeostasis, persistent infection, and cancer surveillance. *Immunol. Rev.* **283**, 54–76 (2018).
- Enamorado, M. et al. Enhanced anti-tumour immunity requires the interplay between resident and circulating memory  $CD8^+$  T cells. *Nat. Commun.* **8**, 16073 (2017).
- Malik, B. T. et al. Resident memory T cells in the skin mediate durable immunity to melanoma. *Sci. Immunol.* **2**, eaam6346 (2017).

14. Murray, T. et al. Very late antigen-1 marks functional tumor-resident CD8 T cells and correlates with survival of melanoma patients. *Front. Immunol.* **7**, 573 (2016).
15. Boddupalli, C. S. et al. Interlesional diversity of T cell receptors in melanoma with immune checkpoints enriched in tissue-resident memory T cells. *JCI Insight* **1**, e88955 (2016).
16. Salerno, E. P., Olson, W. C., McSkimming, C., Shea, S. & Slingluff, C. L. Jr T cells in the human metastatic melanoma microenvironment express site-specific homing receptors and retention integrins. *Int. J. Cancer* **134**, 563–574 (2014).
17. Edwards, J. et al. CD103<sup>+</sup> tumor-resident CD8<sup>+</sup> T cells are associated with improved survival in immunotherapy naive melanoma patients and expand significantly during anti-PD1 treatment. *Clin. Cancer Res.* **24**, 3036–3045 (2018).
18. Mackay, L. K. et al. The developmental pathway for CD103<sup>+</sup> CD8<sup>+</sup> tissue-resident memory T cells of skin. *Nat. Immunol.* **14**, 1294–1301 (2013).
19. Schenkel, J. M., Fraser, K. A., Vezys, V. & Masopust, D. Sensing and alarm function of resident memory CD8<sup>+</sup> T cells. *Nat. Immunol.* **14**, 509–513 (2013).
20. Landsberg, J. et al. Melanomas resist T-cell therapy through inflammation-induced reversible dedifferentiation. *Nature* **490**, 412–416 (2012).
21. Braumüller, H. et al. T-helper-1-cell cytokines drive cancer into senescence. *Nature* **494**, 361–365 (2013).
22. Webb, J. R., Milne, K., Watson, P., Deleeuw, R. J. & Nelson, B. H. Tumor-infiltrating lymphocytes expressing the tissue resident memory marker CD103 are associated with increased survival in high-grade serous ovarian cancer. *Clin. Cancer Res.* **20**, 434–444 (2014).
23. Djenidi, F. et al. CD8<sup>+</sup> CD103<sup>+</sup> tumor-infiltrating lymphocytes are tumor-specific tissue-resident memory T cells and a prognostic factor for survival in lung cancer patients. *J. Immunol.* **194**, 3475–3486 (2015).
24. Wang, B. et al. CD103<sup>+</sup> tumor infiltrating lymphocytes predict a favorable prognosis in urothelial cell carcinoma of the bladder. *J. Urol.* **194**, 556–562 (2015).
25. Komdeur, F. L. et al. CD103<sup>+</sup> tumor-infiltrating lymphocytes are tumor-reactive intraepithelial CD8<sup>+</sup> T cells associated with prognostic benefit and therapy response in cervical cancer. *Oncol Immunology* **6**, e1338230 (2017).
26. Nizard, M. et al. Induction of resident memory T cells enhances the efficacy of cancer vaccine. *Nat. Commun.* **8**, 15221 (2017).
27. Cockburn, I. A. et al. *In vivo* imaging of CD8<sup>+</sup> T cell-mediated elimination of malaria liver stages. *Proc. Natl Acad. Sci. USA* **110**, 9090–9095 (2013).
28. Halle, S. et al. *In vivo* killing capacity of cytotoxic T cells is limited and involves dynamic interactions and T cell cooperativity. *Immunity* **44**, 233–245 (2016).
29. Zhu, J. et al. Immune surveillance by CD8 $\alpha\alpha$ <sup>+</sup> skin-resident T cells in human herpes virus infection. *Nature* **497**, 494–497 (2013); corrigendum 500, 242 (2013).
30. Woon, H. G. et al. Compartmentalization of total and virus-specific tissue-resident memory CD8<sup>+</sup> T cells in human lymphoid organs. *PLoS Pathog.* **12**, e1005799 (2016).

**Acknowledgements** We thank F. Carbone and A. Kallies for critical reading of our manuscript. This work was supported by the University of Melbourne (Elizabeth and Vernon Puzey Scholarship to S.L.P.); the Sylvia and Charles Viertel Charitable Foundation (fellowship to T.G.); the Australian National Health and Medical Research Council (fellowships to L.K.M., R.A.S., J.S.W., S.N.M. and N.D.H.; grants to R.A.S., J.S.W. (1093017) and N.D.H. (1124907, 1124784)); the Cancer Councils of Victoria (grant to N.D.H. (1145730)) and Western Australia (fellowship to J.W.); BHP (grant to J.W.); and the German Research Foundation (GRK2168 Bo&MeRanG Faculty Support Scholarship to M.E., Excellence Cluster ImmunoSensation to M.H. and Program Grant SFB 854/TP27 to T.T.). K.H. is a Rhian and Paul Brazis Fellow in Translational Melanoma Immunology. N.D.H. was supported by the Harry J. Lloyd Charitable Trust, Melanoma Research Alliance, Ian Potter Foundation, Tour de Cure and Cancer Research Institute (USA) and the Victorian State Government Operational Infrastructure Support Scheme.

**Reviewer information** *Nature* thanks A. Goldrath, D. Masopust and D. Speiser for their contribution to the peer review of this work.

**Author contributions** S.L.P., J.R., J.L.H., K.H., N.M., J.E. and R.M. performed experiments. A.B., M.E., T.W., T.T., M.H. and J.W. generated cell lines. S.L.P., U.P., L.K.M., J.W. and T.G. designed experiments. S.L.P., N.M., J.E., U.P. and T.G. analysed data. R.A.S., D.G., S.N.M., N.D.H., J.S.W. and S.B. contributed intellectual input and helped to interpret data. T.G. led the research program. S.L.P. and T.G. wrote the manuscript.

**Competing interests** The authors declare no competing interests.

#### Additional information

**Extended data** is available for this paper at <https://doi.org/10.1038/s41586-018-0812-9>.

**Supplementary information** is available for this paper at <https://doi.org/10.1038/s41586-018-0812-9>.

**Reprints and permissions information** is available at <http://www.nature.com/reprints>.

**Correspondence and requests for materials** should be addressed to L.K.M., J.W. or T.G.

**Publisher's note:** Springer Nature remains neutral with regard to jurisdictional claims in published maps and institutional affiliations.

## METHODS

**Mice.** C57BL/6, gBT-I (ref.<sup>31</sup>), gBT-I × B6.SJL-PtprcaPep3b/BoyJ (gBT-I.CD45.1), gBT-I.Thy1.1, gBT-I.uGFP, OT-I × B6.SJL-PtprcaPep3b/BoyJ (OT-I.CD45.1), *Rag1*<sup>-/-</sup>, *Rag2*<sup>-/-</sup>; *Il2rg*<sup>-/-</sup>, *Il15*<sup>-/-</sup>, *Itgae*<sup>-/-</sup>, *Cd69*<sup>-/-</sup>, *Perf1*<sup>-/-</sup>, *Ifng*<sup>-/-</sup>, *Tnfa*<sup>-/-</sup>, gBT-I.CD45.1 × *Cd69*<sup>-/-</sup>, gBT-I.CD45.1 × *Tnfa*<sup>-/-</sup> and B6(Cg)-*Tyrc*<sup>-2/J</sup> (B6 Albino) mice were bred in the Department of Microbiology and Immunology, The University of Melbourne. gBT-I mice express transgenic T-cell receptors recognizing the HSV glycoprotein-B-derived epitope gB<sub>498–505</sub>, as described<sup>31</sup>. All mice were female and aged between 6–12 weeks at the beginning of experiments. All animal experiments (with a maximum endpoint at a tumour volume of 1,000 mm<sup>3</sup>) were approved by the relevant University of Melbourne Animal Ethics Committee.

**B16 melanoma cell lines.** B16F1-gB.GFP (B16.gB) and B16F10-Ova.GFP (B16.Ova) cells were generated by transduction with retroviral vectors containing a full-length membrane-bound form of HSV gB and enhanced GFP (eGFP), as described<sup>5</sup>. Expression of gB or Ova was confirmed using in vitro activation assays with transgenic T cells, gBT-I or OT-I, respectively. B16.gB cells expressing firefly luciferase (B16.gB.Luc) were generated by transduction of B16.gB cells with retroviruses expressing a puromycin acetyltransferase/luciferase fusion protein (pacLuc2) using the retroviral construct MSCV-ires-pacLuc2, as described<sup>5</sup>. This retroviral construct was provided by S. Baker and R. Williams of St Jude Children's Research Hospital (Memphis, TN, USA). B16.*Tyr*<sup>-/-</sup>.mCherry cells were generated by transfecting B16F1 cells with pX330 expressing a single guide RNA targeting the tyrosinase (*Tyr*) gene (target sequence TGCCTCTCTAAGAAGCTTGT). Single-cell clones were established and successful genome editing of the tyrosinase gene was verified by next-generation sequencing using the MiSeq platform. A clone (D8) with 1-nucleotide insertions in all alleles was selected and designated as B16.*Tyr*<sup>-/-</sup>. B16.*Tyr*<sup>-/-</sup>.mCherry or B16.mCherry cells were established by retroviral transduction with pRp-mCherry and subsequently expanded as a polyclonal culture. Subsequently, B16.*Tyr*<sup>-/-</sup>.mCherry or B16.mCherry cells were transduced with retroviral vectors containing full-length membrane bound gB and eGFP to yield B16.gB.*Tyr*<sup>-/-</sup>.mCherry or B16.gB.mCherry cells, respectively. All B16 cell lines tested negative for mycoplasma contamination and were cultured and passaged in RPMI medium containing 10% fetal calf serum (FCS), L-glutamine (4 mM ml<sup>-1</sup>), penicillin (1,000 units per ml), streptomycin (2 mg ml<sup>-1</sup>) and 2-mercaptoethanol (1 mM l<sup>-1</sup>) at 37°C/6.5% CO<sub>2</sub>.

**B16 melanoma inoculation and viral infection.** For B16 melanoma inoculation, mice were anaesthetized with a 1/1 mixture of ketamine (100 mg kg<sup>-1</sup>, Parnell Laboratories) and xylazil (Troy Laboratories) by intraperitoneal injection, and lubricating eye gel (Allergen Australia) was applied to the eyes to prevent drying. Mice were shaved (with a Wahl razor) and depilated using Veet cream (Reckitt Benckiser). B16 melanoma cells were harvested by washing with PBS, then incubating cells at 37°C for 3–5 min with 1 × trypsin/EDTA solution (Sigma) and washing with Hanks' balanced saline solution (HBSS). For subcutaneous B16 inoculation, 1 × 10<sup>5</sup> B16.gB cells were suspended in 50 µl HBSS and injected under the left flank using a 30G needle. For epicutaneous inoculation, left flank skin was lightly abraded by application of a power tool with grindstone attachment (Dremel) for 10–15 s with constant rotation, and the scarified site was wiped with a cotton tipped applicator (Livingstone) soaked in PBS. B16.gB cells (1 × 10<sup>5</sup>) were suspended in 10 µl Matrigel basement membrane matrix (Corning) and applied to the scarified region. Mice were rested for about 10 min to allow solidification of Matrigel before application of Op-site Flexigrid (Smith and Nephew) over the gel. Mice were bandaged by wrapping micropore and transpore surgical tape (3M) around the torso and bandages were removed 4 days later. Developing tumours were measured using a digital caliper and volume estimated using the formula: volume = ((width<sup>2</sup> × length)/2). HSV infections were performed by scarification using 1 × 10<sup>6</sup> plaque-forming units of the KOS strain of HSV-1, as described<sup>32</sup>.

**Flow cytometry.** Lymphocytes were isolated from the spleen and lymph nodes by grinding organs through a metal mesh to create single-cell suspensions. T cells were isolated from the skin as described<sup>18</sup>. Briefly, skin was incubated in Dispase solution (Roche, 2.5 mg ml<sup>-1</sup>) for 90 min and the epidermis separated from the dermis. The dermis was finely chopped and incubated in collagenase type III (Worthington, 3 mg ml<sup>-1</sup>) and the epidermis placed in trypsin/EDTA (Sigma) and incubated at 37°C for 30 min. Alternatively, skin was incubated in liberase TL research grade solution (Sigma, 0.25 mg ml<sup>-1</sup>) for 20 min and the epidermis separated from the dermis then chopped in liberase TL research grade solution (Sigma, 0.25 mg ml<sup>-1</sup>) and incubated for a further 60 min. T cells were isolated from tumours by placing melanomas in collagenase type III, chopping with scissors, incubating samples at 37°C for 90 min then grinding tissue through a 70-µm nylon filter to create a single-cell suspension. Tumour-cell suspensions were treated with red blood cell lysis buffer (Sigma) before staining.

For in situ cytokine-production assays, mice were injected with 100 µg of gB or OVA peptide diluted in PBS containing 0.25 mg ml<sup>-1</sup> brefeldin A (BFA, Sigma Aldrich) for 4–5 h before organ harvest. Skins and tumours were processed as normal in dispase and collagenase containing 0.02 µg BFA. Cells were stained

with antibodies and their expression of markers determined using a BD Fortessa (BD Biosciences) and analysed using Flowjo 9 (Treestar). Antibodies used were: anti-mouse CD45.1 (A20), CD45.2 (104), CD8α (53-6.7), Vα2 (B20.1), CD69 (H1.2F3), CD16/CD32 (2.4G2), CD44 (IM7), CD62L (MEL-14), PD-1 (J43), IFN-γ (XMG1.2), TNF (MP6-XT22) from BD Biosciences; anti-mouse CD45.1 (A20), CD8α (53-6.7), CD103 (2E7), KLRG1 (2F1), PD-1 (J43) from eBiosciences/ThermoFisher Scientific; and anti-mouse CD45.2 (104), CD103 (2E7), CD8α (53-6.7), Thy1.1 (OX-7), CD69 (H1.2F3) and PD-1 (29F.1A12) from Biolegend. For in situ cytokine assays, samples were fixed and stained for intracellular cytokines using a Foxp3/transcription-factor-staining buffer kit according to the manufacturer's instructions (eBioscience). Cell viability was determined using either a fixable LIVE/DEAD near-infrared cell-staining kit (BD Biosciences) or fixable Zombie Aqua or Zombie Yellow kits (Biolegend). Cells were enumerated by adding SPHERO calibration particles (BD Biosciences) to each sample before acquisition using a BD Fortessa II, or sorted using a BD FACS Aria III (both BD Biosciences).

**Quantitative real-time PCR.** RNA was extracted from sorted samples using a RNeasy micro kit (Qiagen) or Direct-Zol RNA microprep kit (Zymo Research) and then converted to complementary DNA using a high-capacity cDNA reverse transcription kit (ThermoFisher Scientific) according to the manufacturer's instructions. Genes of interest were preamplified from cDNA using Taqman gene-expression assays: *Ctla4* (Mm00486849\_m1), *Pdcd1* (Mm01285676\_m1), *Lag3* (Mm00493071\_m1), *Tigit* (Mm03807533\_m1) and Taqman preamp master mix (Life Technologies). Real-time quantitative PCR was performed with the same Taqman gene-expression assays and Taqman fast advanced master mix (Life Technologies) using a Quantasoft 7 real-time PCR machine (ThermoFisher Scientific). Cycle-threshold values were determined for each gene and normalized to the housekeeping genes *Hprt* (Mm00446968\_m1), *Gapdh* (Mm99999915\_g1) and *Tbp* (Mm00446973\_m1).

**Intravital two-photon microscopy.** Mice were anaesthetized with isoflurane (Cenvet: 2.5% for induction, 1–1.5% for maintenance) vaporized in an 80/20 mixture of O<sub>2</sub> and air, and shaved on the left flank, with hair depilated using Veet; then surgery was performed as described<sup>6</sup>. Briefly, two incisions were made along the left flank approximately 2–2.5 cm apart either side of the tumour or Dremel site, and the skin was separated from the peritoneum using scissors. An 18-mm-wide piece of 1-mm stainless steel was inserted between the peritoneum and dermis to form a stable raised platform that was attached to a custom-made imaging platform. The dermis was adhered to the stainless-steel platform with Vetbond tissue adhesive (3M). Vacuum grease (Dow Corning) was applied at the edges of the skin and a glass coverslip was placed over the skin and sealed using the vacuum grease. Incision sites were regularly irrigated with PBS to prevent dehydration of the peritoneum during imaging. Images were acquired with an upright FV-MPERS (Olympus) multiphoton microscope with a 25 × /1.05NA water-immersion objective enclosed in a heated chamber maintained at 35°C. Fluorescence excitation was provided with Mai-Tai (690–1,040 nm) and Insight (680–1,300 nm) lasers. mCherry was excited at 1,100 nm, and eGFP and collagen (visualized by second harmonic generation, SHG) were excited at 950 nm. For four-dimensional data sets, three-dimensional stacks were captured at a resolution of 512 × 512 pixels every 60–75 s over a period of 1–2 h with 2.5–3.5-µm intervals. Raw imaging data were processed, and movies were generated in Imaris 8 or Imaris 9 (Bitplane) and edited using Adobe After Effects.

**Intravenous and epicutaneous T-cell transfer.** For adoptive T-cell transfer, naive gBT-I.CD45.1, gBT-I.Thy1.1 or gBT-I.uGFP T cells were isolated from lymph nodes of donor mice and 0.5 × 10<sup>5</sup> to 1 × 10<sup>5</sup> cells injected intravenously into recipient mice at least 1 day before B16 melanoma inoculation or HSV infection. For epicutaneous T-cell transfer or intravenous transfer of in vitro activated CD8<sup>+</sup> T cells, transgenic gBT-I.CD45.1, gBT-I.Thy1.1 or OT-I.CD45.1 T cells were activated in vitro for 4–5 days with gB<sub>498–505</sub> (SSIEFARL) or OVA<sub>257–264</sub> (SIINFEKL) peptide-pulsed splenocytes in the presence of recombinant human interleukin (IL)-2 (25 units per ml, Peprotech), as described<sup>8</sup>. Activated transgenic T cells suspended in Matrigel basement membrane matrix solution (1 × 10<sup>6</sup> cells per 10 µl) were transferred in an identical manner to that described above for epicutaneous B16 melanoma cell inoculation, except that a total of 4 × 10<sup>6</sup> T cells were transferred to mice by application of 4 × 10<sup>6</sup> µl of Matrigel cell suspension to four adjacent abrasion sites arranged in a cloverleaf shape. For transfer of in vitro activated CD8<sup>+</sup> T cells for qPCR experiments, gBT-I cells (10 × 10<sup>6</sup>) were injected intravenously into recipient mice bearing macroscopic melanoma tumours.

**In vivo bioluminescence imaging.** Mice were injected intraperitoneally with 150 mg per kg of D-luciferin potassium salt (ThermoFisher Scientific) in PBS and left to rest for 5 min, before being anaesthetized with isoflurane (Cenvet: 2.5%) vaporized in an 80/20 mixture of O<sub>2</sub> and air, shaved on the left flank and depilated using Veet cream, as described above. Images were acquired using an IVIS Lumina XRMS series III imaging system (Perkin Elmer) with an exposure of 300 s. Images were analysed with Living Image v4.4 software.

**Genomic DNA extraction and ddPCR.** Tumours, non-developer skin corresponding to the abraded site or untreated skin were harvested and placed in 0.5-ml polypropylene tubes containing 1.4-mm ceramic beads (soft tissue homogenizing mix, Omni) and DNA lysis buffer (50 mM Tris, 50 mM EDTA, 1% SDS in MilliQ H<sub>2</sub>O, pH8). Tissues were homogenized by 2 × 30 s rounds of shaking in a Bead Ruptor 24 Elite (Omni) at a speed of 8 m s<sup>-1</sup> and digested overnight with proteinase-K (12 milli arbitrary units, Qiagen) at 55 °C in a shaking incubator. The lysate was mixed with ice-cold ammonium acetate (7.5 M), and then tubes were centrifuged and genomic DNA extracted by mixing the supernatant with 100% isopropanol and washing the DNA pellet with 70% ethanol/MilliQ H<sub>2</sub>O solution. DNA pellets were resuspended in Tris/EDTA buffer (pH 8) and passed through a DNeasy spin column (Qiagen). ddPCR reactions comprised about 3–10% of total extracted gDNA (415 ng DNA per well × 4 wells per sample), ddPCR supermix for probes (BioRad), *Hind*III enzyme (5 IU per well, New England BioLabs), forward/reverse primers (900 nM) and probes (250 nM) specific for *luc* or *gB* and *Vim*. Droplets were generated and read using a QX200 AutoDG droplet digital PCR System and a C1000 Touch thermal cycler (all BioRad) according to the manufacturer's instructions. Primers and probes were purchased from Integrated DNA Technologies (*Luc*, forward: 5'-GACACCGGTAAGACACTGGG-3', reverse: 5'-GCCTCGGGGTTGTTAACGTA-3', probe: 5'-FAM/GCGTCCGTG/ZEN/GCCCATGATC/3IAbkFQ-3'; and *Vim*, forward: 5'-AGCTGCTAACTACCAGGACACTATTG-3', reverse: 5'-CGAAGGTGACGAGCCATCTC-3', probe: 5'-HEX/CCTTCATGT/ZEN/TTTGGATCTCATCTGCAGG/3IAbkFQ-3') or Life Technologies (HSV-gB, forward: 5'-GCAGTACTACCTGGCCAATGG-3', reverse: 5'-CGCGAGCGTGTGGTCT-3', probe: 5'-FAM/ATCGCGTACCAGCCCC/NFQ-3'). *Vim* quantification was used as a housekeeping positive control. Data were analysed using QuantaSoft Software V1.7 (BioRad).

**Human melanoma samples.** The human melanoma samples ( $n = 68$  for lymph nodes;  $n = 3$  for skin) were obtained from The Melanoma Institute Australia biopsied specimen bank with written informed patient consent and institutional review board approval (The Sydney Local Health District Human Research Ethics Committee, protocol numbers X15-0454 and HREC/11/RPAH/444). Their analysis was undertaken in accordance with the National Health and Medical Research Council of Australia's National Statement on Ethical Conduct in Human Research. Patients were selected on the basis of clinical and pathological confirmation of cutaneous melanoma (mucosal and acral melanomas excluded), and all patients had not received any systemic treatment or radiotherapy in the biopsied area before surgery. All samples analysed in this study were from lymph-node or skin metastases and a detailed clinical overview of all the patients has been described previously<sup>17</sup>. Images displayed in Fig. 2 were taken from two representative patient samples with the following characteristics—patient 1, age: 56, gender: male, site: lymph node; and patient 2, age: 77, gender: female, site: subcutaneous skin.

**Multiplex immunofluorescence microscopy on human tissue.** Melanoma paraffin-embedded tissue sections were first deparaffinized, rehydrated, and treated with heat-induced antigen-retrieval buffer (pH 9). All staining was performed on a Dako autostainer. Briefly, sections were incubated with 3% hydrogen peroxide for 10 min at room temperature, and then incubated with a single primary antibody (against CD8 (Ab4055), CD103 (EPR4166(2)) or Sox10 (Biocare-BC34)) made up in Da Vinci green diluent solution (Biocare Medical) for 35 min. Sections were then washed and incubated with a probe antibody (rabbit or mouse MACH3 probe, Biocare Medical) specific to the species of the primary antibody for 10 min, washed and then incubated for a further 10 min with a horseradish-peroxidase

(HRP)-conjugated antibody (rabbit or mouse MACH3 HRP, Biocare Medical) specific to the probe. Following this, sections were washed and then incubated with opal fluorophores at a 1/50 dilution made up in tyramide signal amplification (TSA) reagent (Opal 7-Colour IHC, Perkin Elmer, USA). Between subsequent staining runs, tissues were boiled in pH 9 antigen-retrieval buffer to strip the primary antibody complex from the sample. Single-colour controls were set up alongside the test panel in order to determine background fluorescence and nonspecific binding. Images were taken using a standard fluorescent microscope fitted with an automated quantitative pathology system (Vectra) in conjunction with Vectra 3.3 and inForm 2.3.0 software (Perkin Elmer).

**Dinitrofluorobenzene treatment.** Mice were shaved and depilated before application of 15  $\mu$ l of dinitrofluorobenzene (DNFB, 0.25%) in acetone and oil (4/1) to a 1.5-cm<sup>2</sup> region of skin on the same day as *in vitro* activated T-cell transfer.

**Depletion of gBT-I.Thy1.1 T cells.** To deplete circulating gBT-I.Thy1.1 cells, we injected mice intraperitoneally 2–4 times with 0.5–1  $\mu$ g anti-mouse/rat Thy1.1 monoclonal antibody (anti-Thy1.1, clone HIS51; eBioscience) in PBS more than 30 days after gBT-I cell transfer; the mice then rested for at least 7 days before subsequent tumour challenge. Depletion of circulating gBT-I.Thy1.1 cells was confirmed by flow cytometric analysis of blood samples from the tail vein of mice more than 7 days after depletion. For depletion of skin gBT-I.Thy1.1 cells, mice were injected intradermally with 2 × 10  $\mu$ g and 1 × 5  $\mu$ g doses of anti-Thy1.1 antibody diluted in PBS (100  $\mu$ l total volume) using a 30G needle over 3 days, with a second round of intradermal anti-Thy1.1 injections occurring more than 30 days after the initial treatment phase. Control mice received PBS alone.

**Statistics and reproducibility.** Two-tailed Mann–Whitney U-tests and Mantel–Cox tests were used where indicated. Numerical values stated in the main text are given as the mean  $\pm$  standard error of the mean (s.e.m.). All statistical analyses were performed in Prism 7 (Graphpad) and are two-sided. The experiments were not randomized and the investigators were not blinded to allocation during experiments and outcome assessment. No statistical methods were used to pre-determine sample size. All experiments were performed at least twice, either with similar results obtained and representative data shown, or with pooled data shown. Survival curves, dotted bar graphs and pie charts with pooled data from multiple experiments include all experiments performed. Photographs are representative of at least three biologically independent experiments repeated with similar results. Bioluminescence imaging data are from two biologically independent experiments. Where representative histograms are shown, data reflect at least two independent experiments with at least four mice per experiment, in which similar results were obtained.

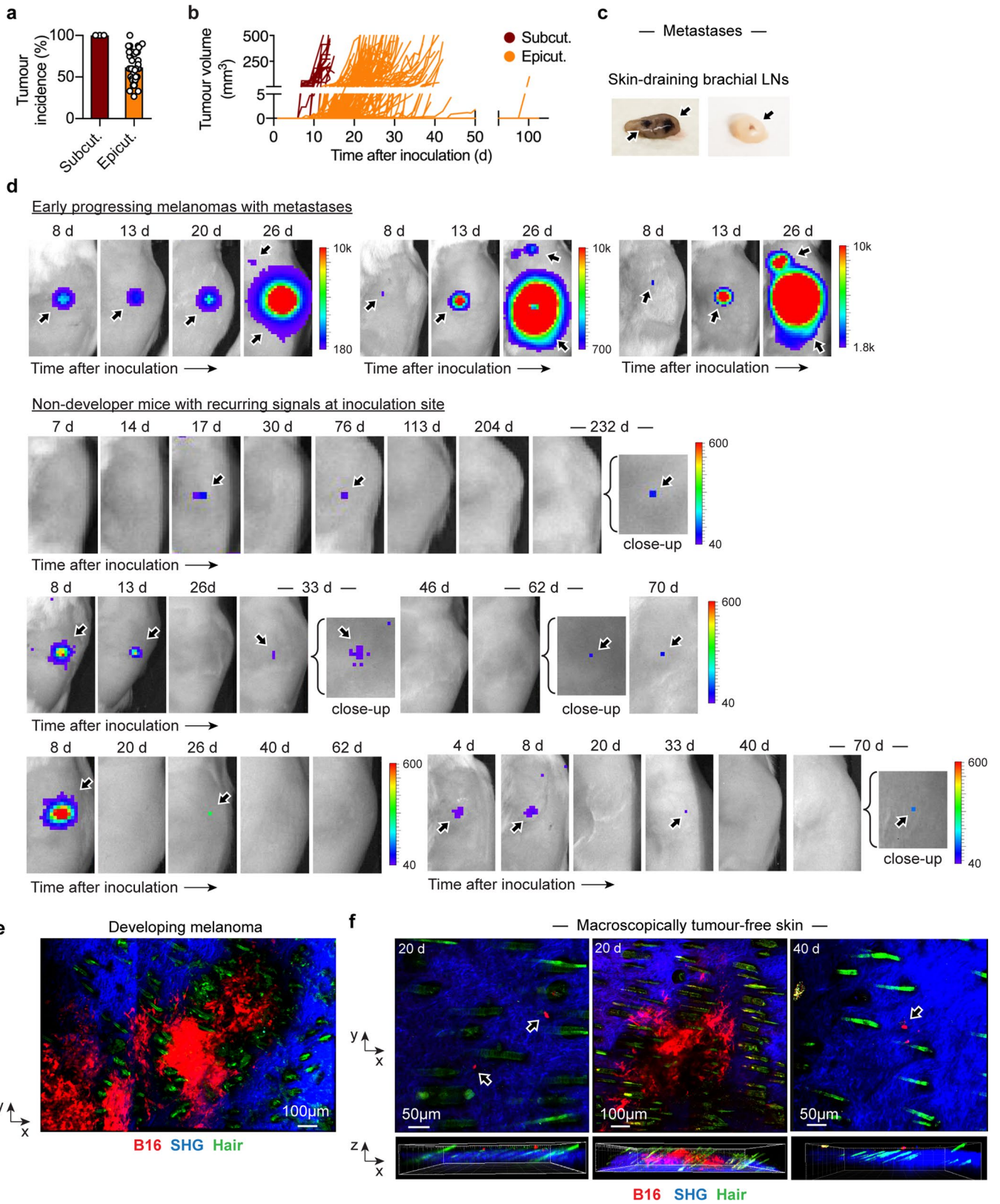
**Reporting summary.** Further information on experimental design is available in the Nature Research Reporting Summary linked to this paper.

## Data availability

The data that support the findings of this study are available from the corresponding authors upon reasonable request.

- Mueller, S. N., Heath, W., McLain, J. D., Carbone, F. R. & Jones, C. M. Characterization of two TCR transgenic mouse lines specific for herpes simplex virus. *Immunol. Cell Biol.* **80**, 156–163 (2002).
- van Lint, A. et al. Herpes simplex virus-specific CD8<sup>+</sup> T cells can clear established lytic infections from skin and nerves and can partially limit the early spread of virus after cutaneous inoculation. *J. Immunol.* **172**, 392–397 (2004).

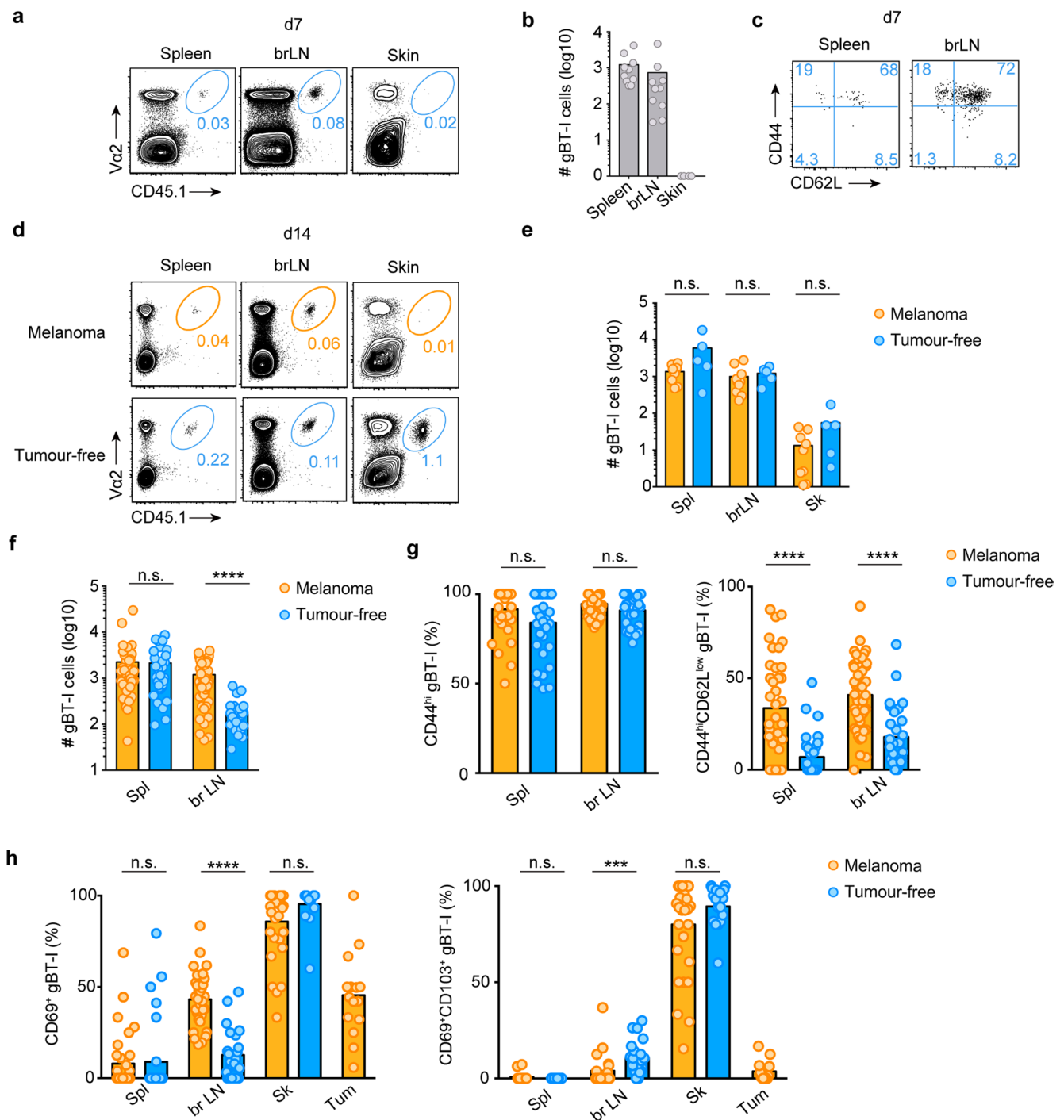




Extended Data Fig. 1 | See next page for caption.

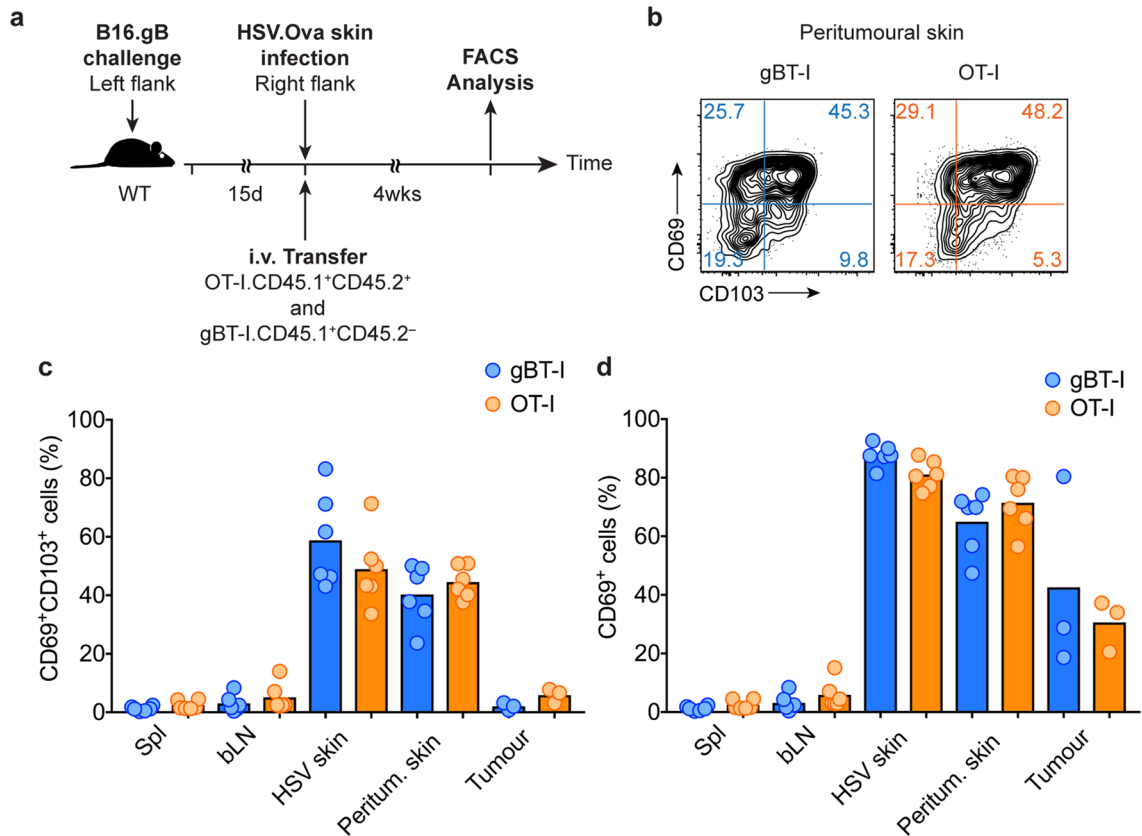
**Extended Data Fig. 1 | Growth kinetics and persistence of B16.gB cells after e.c. inoculation.** **a**, Rate of tumour incidence across individual experiments after s.c. (Subcut.) and e.c. (Epicut.) inoculation with either B16.gB or B16.gB.Luc cells in WT mice. Data pooled from  $n = 3$  (s.c.) and  $n = 46$  (e.c.) biologically independent experiments with  $n = 15$  (s.c.) or  $n = 452$  (e.c.) mice. **b**, Tumour growth kinetics after s.c. or e.c. inoculation with B16.gB or B16.gB.Luc cells. Data pooled from  $n = 3$  biologically independent experiments with  $n = 15$  mice (s.c.) or  $n = 22$  independent experiments with  $n = 154$  mice (e.c.). **c**, Photographs of metastases in tumour-draining brachial lymph nodes (LNs) of mice with progressive melanoma following e.c. B16.gB inoculation. Representative of  $n = 46$  biologically independent experiments. **d**, B6 albino mice were inoculated

epicutaneously with B16.gB.Luc cells and subjected to longitudinal bioluminescence imaging. Bioluminescence signals (arrows) emitted from progressing melanomas or from skin of non-developer mice. Data representative of  $n = 2$  biologically independent experiments with  $n = 18$  mice. **e**, Two-photon microscopy image of a macroscopic melanoma 2 or more weeks after e.c. inoculation with B16.*Tyr*<sup>-/-</sup>.mCherry cells. **f**, Two-photon microscopy images of macroscopically tumour-free skin with persistent B16.*Tyr*<sup>-/-</sup>.mCherry cells (arrows) at indicated times post-inoculation. **e, f**, B16.*Tyr*<sup>-/-</sup>.mCherry (B16) cells, red; SHG, blue. Note autofluorescent hair (green). Data representative of  $n = 3$  biologically independent experiments with  $n = 22$  mice.



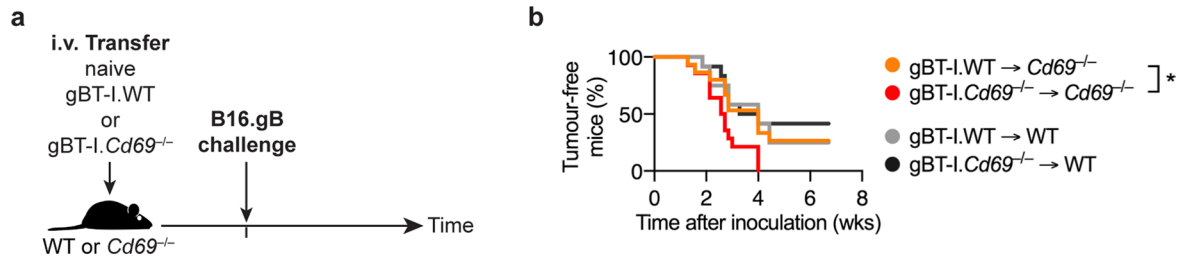
**Extended Data Fig. 2 | Responses of gBT-I cells to e.c. inoculation with B16.gB cells.** WT mice were transferred with naive gBT-I.CD45.1 cells before e.c. inoculation with B16.gB cells. **a**, Detection of gBT-I cells (blue ovals; based on expression of CD45.1 and the T-cell-receptor chain Vα2) in spleen, tumour-draining brachial lymph nodes (brLN) and tumour-challenged skin at 7 days (d7) post-inoculation. **b, c**, Number (**b**) and phenotype (**c**) of gBT-I cells shown in panel **a**. Data representative of (**a, c**) or pooled from (**b**)  $n = 2$  biologically independent experiments with  $n = 10$  mice. **d**, Detection of gBT-I.CD45.1 cells in the indicated organs from developer ('Melanoma') and non-developer ('Tumour-free') mice at 14 days post-inoculation. Data representative of

$n = 2$  biologically independent experiments with  $n = 10$  mice. **e**, Number of gBT-I.CD45.1 cells isolated from the indicated organs of developer ('Melanoma') and non-developer ('Tumour-free') mice 14 days post-inoculation. Data pooled from  $n = 2$  biologically independent experiments with  $n = 10$  (Melanoma) or  $n = 5$  (Tumour-free) mice. **f–h**, Number (**f**) and phenotype (**g, h**) of gBT-I.CD45.1 cells isolated from the indicated organs of developer ('Melanoma') and non-developer ('Tumour-free') mice more than 21 days post-inoculation. Data pooled from  $n = 5$  biologically independent experiments with  $n = 83$  mice. \*\*\* $P = 0.0006$ , \*\*\*\* $P < 0.0001$ , Mann–Whitney test.



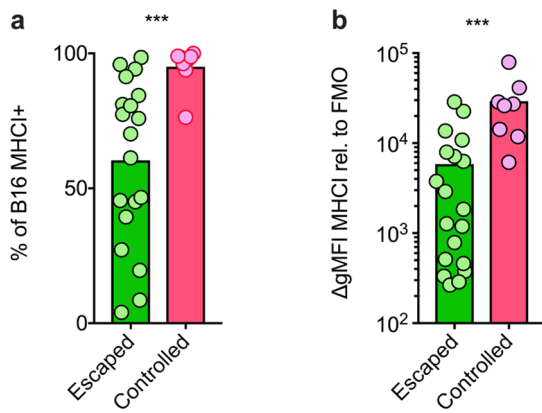
**Extended Data Fig. 3 | Generation of melanoma-associated  $T_{RM}$  cells does not require local antigen.** **a**, Experimental protocol. WT mice were inoculated epicutaneously with B16.gB cells on the upper left flank and monitored for tumour progression. Mice developing macroscopic melanoma were co-transferred intravenously (i.v.) with equal numbers of naive gBT-I.CD45.1 cells and OT-I.CD45.1.CD45.2 cells, and challenged with HSV.Ova on the lower right flank. Tissues were harvested for

fluorescence-activated cell sorting (FACS) analysis 4 weeks after HSV infection. **b**, Surface phenotype of gBT-I or OT-I cells isolated from peritumoural skin 4 weeks after HSV infection. **c**, **d**, Proportion of gBT-I or OT-I cells expressing CD69 and CD103 (**c**) or CD69 only (**d**) in the indicated organs (Spl, spleen; Peritum, peritumoural). Data are representative of (**b**) or pooled (**c**) from one experiment with  $n = 6$  mice.

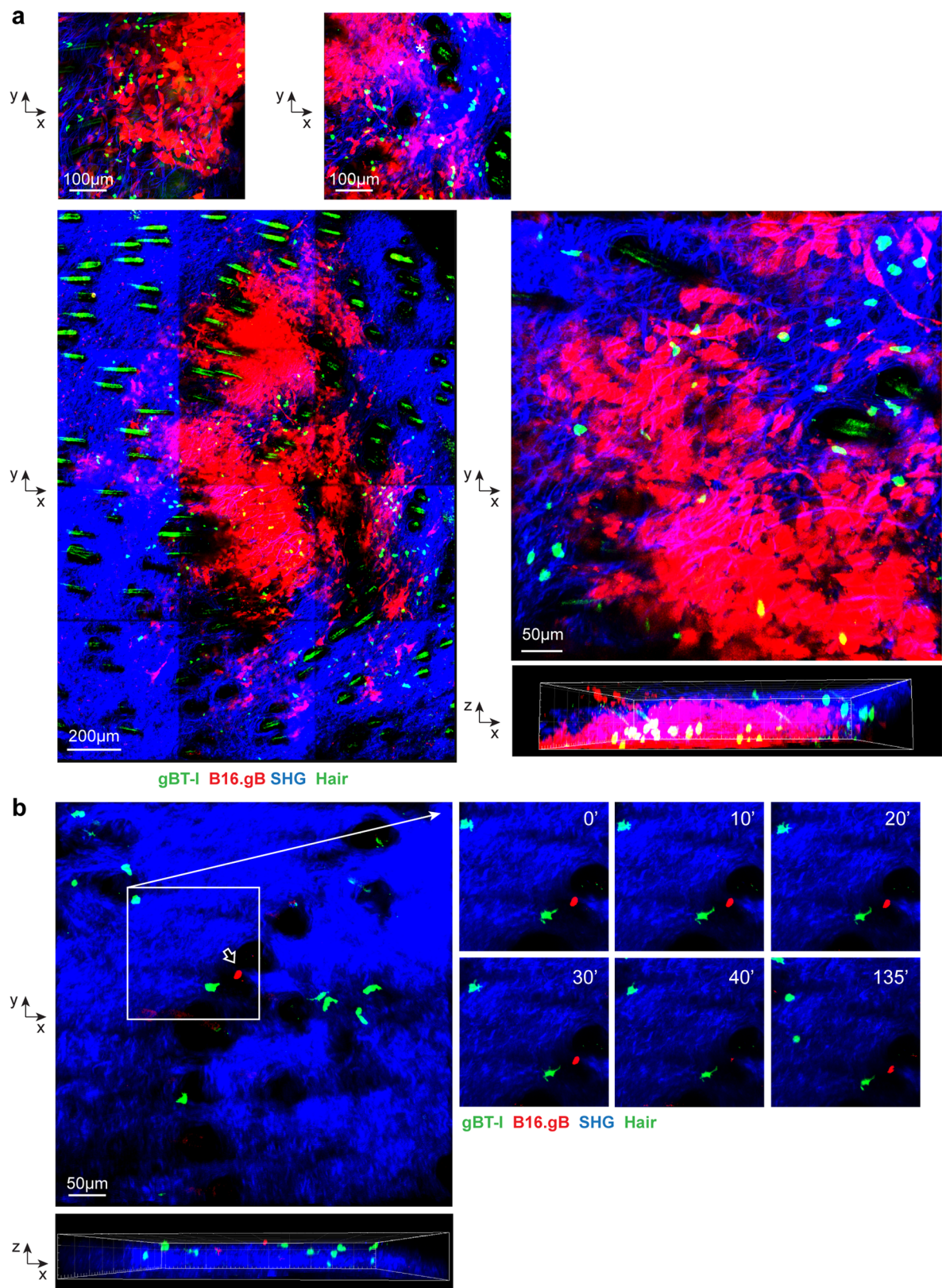


**Extended Data Fig. 4 | gBT-I.WT cells can rescue the melanoma-protection defect in *Cd69*<sup>-/-</sup> mice.** **a**, WT or *Cd69*<sup>-/-</sup> mice were transferred naive gBT-I.WT or gBT-I.*Cd69*<sup>-/-</sup> ( $1 \times 10^5$ ) cells, then inoculated epicutaneously with B16.gB cells and monitored for tumour development. **b**, Proportion of tumour-free non-developer WT (grey and

black) or *Cd69*<sup>-/-</sup> (coloured) mice following tumour inoculation over time. Data pooled from  $n = 2$  biologically independent experiments with  $n = 12$  (gBT-I.WT→WT, gBT-I.*Cd69*<sup>-/-</sup>→WT),  $n = 14$  (gBT-I.*Cd69*<sup>-/-</sup>→*Cd69*<sup>-/-</sup>) or  $n = 15$  (gBT-I.WT→*Cd69*<sup>-/-</sup>) mice per group. \* $P = 0.0217$ , log-rank Mantel Cox test.

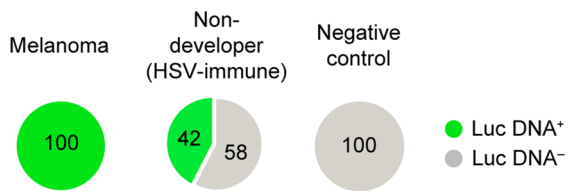


**Extended Data Fig. 5 | MHC I expression by progressing or controlled melanoma.** **a**, WT mice were transferred naive gBT-I.CD45.1 cells and inoculated epicutaneously with B16.gB.*Tyr*<sup>-/-</sup>.mCherry cells. Tumours isolated from mice with progressively growing melanomas (defined by an increase in tumour volume over at least four consecutive days; 'escaped') or tumours that remained small and did not progress (defined by a stable tumour volume over a period of 1.5–3 weeks; 'controlled') were harvested and analysed by flow cytometry. **a**, Proportion of B16.gB.*Tyr*<sup>-/-</sup>.mCherry cells isolated from escaped or controlled tumours that expressed MHC class I (H2-K<sup>b</sup>) proteins at the time of harvest. \*\*\* $P = 0.0003$ . **b**, Geometric mean fluorescence intensity (gMFI) of MHC I expression by B16.gB.*Tyr*<sup>-/-</sup>.mCherry cells isolated from escaped or controlled tumours, normalized to the gMFI of fluorescence minus one (FMO) controls. \*\*\* $P = 0.0005$ . Data in **a**, **b** pooled from  $n = 3$  biologically independent experiments with  $n = 19$  (escaped) or  $n = 8$  (controlled) mice. Mann-Whitney test.



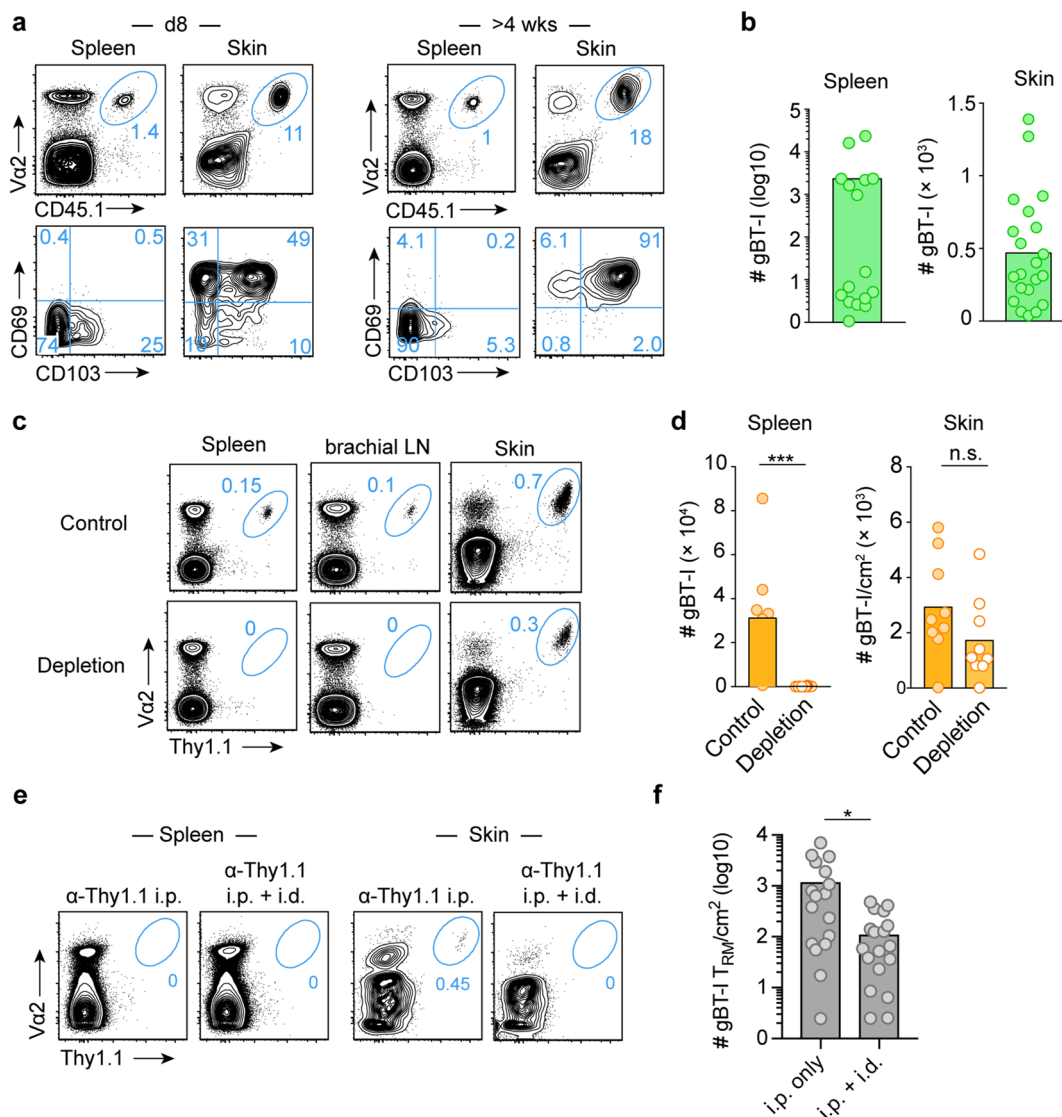
**Extended Data Fig. 6 | Tumour-primed gBT-I.uGFP cells survey developing and persistent melanoma in skin.** B6 albino mice were transferred naive gBT-I.uGFP cells and inoculated epicutaneously with B16.gB.*Tyr*<sup>-/-</sup>.mCherry cells. **a**, Two-photon microscopy images depicting localization of gBT-I.uGFP cells around a B16.gB.*Tyr*<sup>-/-</sup>.mCherry tumour (red) in the skin of mice developing macroscopic melanoma. **b**, Representative two-photon microscopy image and time-lapse series

(minutes, ') of gBT-I.uGFP cells in proximity to persistent B16.gB.*Tyr*<sup>-/-</sup>.mCherry cells in the skin of a non-developer mouse. **a**, **b**, Red, B16.gB.*Tyr*<sup>-/-</sup>.mCherry cells (B16.gB; arrows); green, gBT-I.uGFP cells (gBT-I); blue, SHG. Note autofluorescent hair (green). Data in **a** and **b** are representative of  $n = 3$  biologically independent experiments with  $n = 17$  mice.



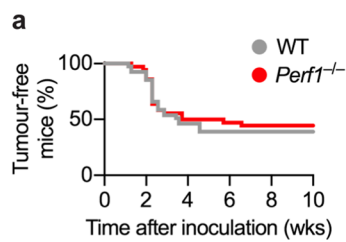
**Extended Data Fig. 7 | Detection of B16-derived genomic DNA in skin of HSV-immune non-developer mice.** Frequency of luciferase (Luc) gDNA detection by ddPCR in the skin of previously naive mice developing macroscopic melanoma (a positive control), HSV-immune non-developer mice, or naive mouse skin (negative control) more than 4 weeks after e.c. inoculation with B16.gB.Luc cells. Data pooled from  $n = 2$  biologically independent experiments with  $n = 17$  (HSV),  $n = 6$  (naive skin) or  $n = 2$  (melanoma) mice.



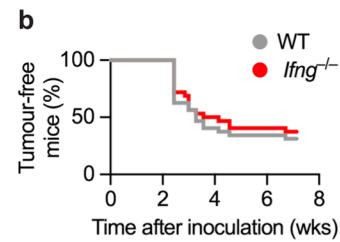


**Extended Data Fig. 8 | Generation of  $T_{RM}$  cells by localized deposition, and antibody strategies for selective  $T_{CIRC}$  or  $T_{RM}$  depletion.** WT mice received activated gBT-I.CD45.1 or gBT-I.Thy1.1 cells ( $1 \times 10^6$  or  $4 \times 10^6$ ) by e.c. transfer. **a**, Frequency and phenotype of transferred  $V\alpha 2^+$  gBT-I.CD45.1 cells in the spleen and skin at 8 days and more than 4 weeks after transfer. Data representative of  $n = 2$  biologically independent experiments with  $n = 10$  mice (day 8) and  $n = 8$  mice (more than 4 weeks). **b**, Number of gBT-I.CD45.1 cells isolated from spleen and skin more than 4 weeks after transfer, determined by flow cytometry. Data pooled from  $n = 5$  biologically independent experiments with  $n = 21$  mice. **c**, **d**, Frequency (**c**) and number (**d**) of e.c. transferred gBT-I.Thy1.1 cells isolated from the indicated organs more than 7 days

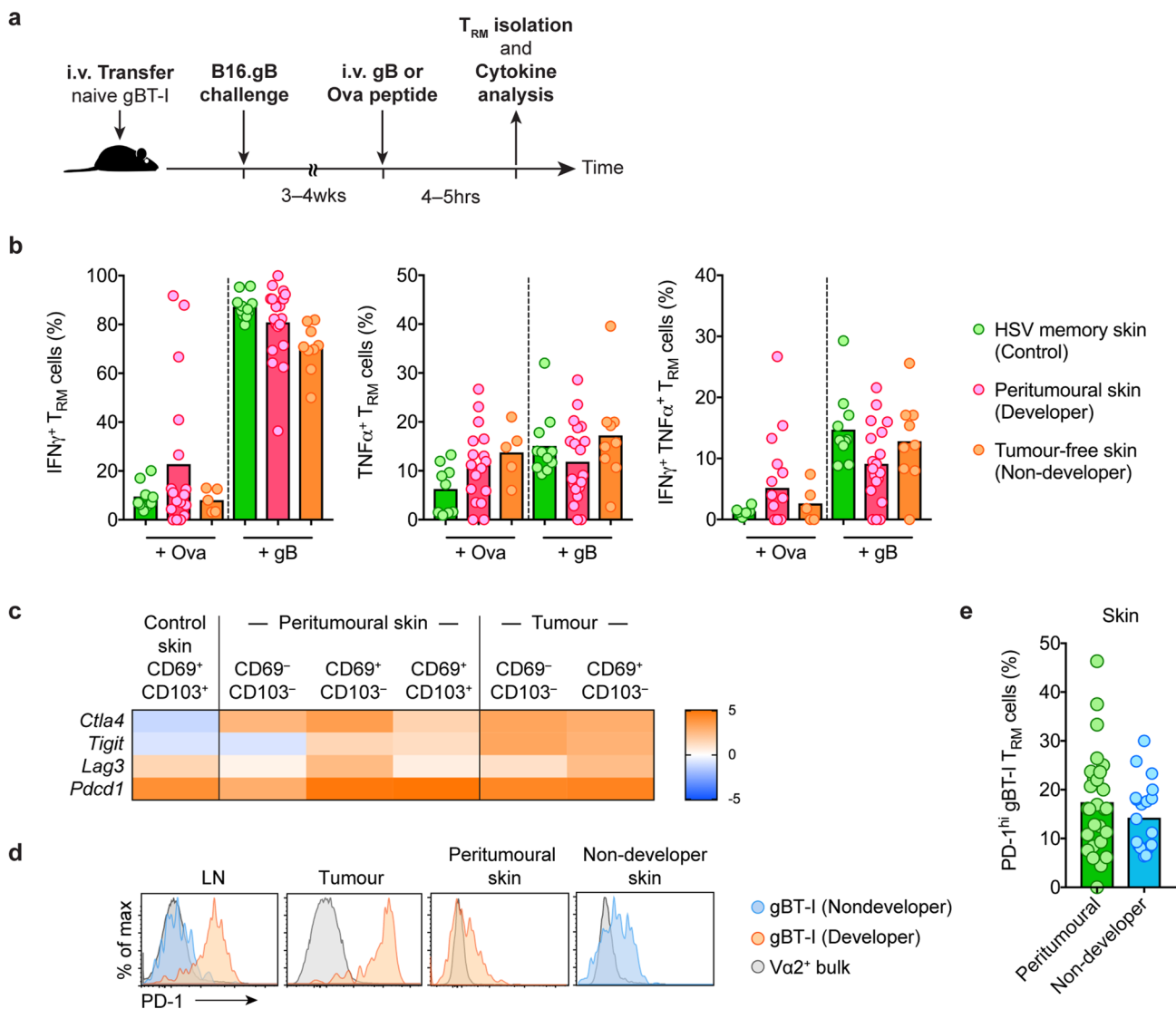
after intraperitoneal (i.p.) treatment with PBS ('Control') or anti-Thy1.1 antibody ('Depletion'). Data representative of (**c**) or pooled from (**d**)  $n = 2$  biologically independent experiments with  $n = 9$  mice per group.  $***P = 0.0002$ , Mann-Whitney test. **e**, **f**, Frequency (**e**) and number (**f**) of e.c. transferred gBT-I.Thy1.1 cells in the spleen and skin more than 50 days after i.p. treatment with low-dose anti-Thy1.1 antibody and intradermal (i.d.) treatment with high-dose anti-Thy1.1 antibody or PBS. Data representative of (**e**) or pooled from (**f**)  $n = 4$  biologically independent experiments with  $n = 20$  (i.p. only) or  $n = 22$  (i.p. + i.d.) mice. Only values greater than zero are plotted on the logarithmic scale.  $*P = 0.0261$ , Mann-Whitney test.



**Extended Data Fig. 9 | Tumour incidence in mice genetically deficient in perforin or IFN- $\gamma$  production.** **a**, Proportion of tumour-free non-developer WT or perforin-deficient *Per1*<sup>-/-</sup> mice after e.c. inoculation with B16.gB cells. **b**, Proportion of tumour-free non-developer WT or



IFN- $\gamma$ -deficient (*Ifng*<sup>-/-</sup>) mice following e.c. inoculation with B16.gB cells. Data pooled from  $n = 4$  (**a**) or  $n = 3$  (**b**) biologically independent experiments with  $n = 36$  (*Per1*<sup>-/-</sup>) or  $n = 41$  (WT) mice (**a**) or  $n = 32$  mice per group (**b**).



**Extended Data Fig. 10 | Cytokine production and expression of inhibitory receptors by melanoma-associated T<sub>RM</sub> cells.** **a**, WT mice were transferred naive gBT-I.CD45.1 (gBT-I) cells and e.c. inoculated with B16.gB cells. A separate group of mice received naive gBT-I.CD45.1 cells followed by skin infection with HSV (not shown). Three to four weeks after tumour or viral challenge, mice were i.v. injected with either gB or Ova peptide and brefeldin A, and organs were harvested for flow cytometric analysis 4–5 hours later. **b**, Proportion of gBT-I cells expressing the indicated cytokines (IFN- $\gamma$  and TNF- $\alpha$ ) isolated from HSV-challenged skin (green), peritumoural skin from developer mice (pink) or tumour-free skin of non-developer mice (orange) administered either gB or Ova peptide. **c**, In vitro activated gBT-I.CD45.1 cells were transferred to WT mice bearing macroscopic B16.gB tumours or to a separate group of previously naive mice that were then treated with DNFB on skin to facilitate T<sub>RM</sub> generation. Two weeks later, populations of CD69<sup>+</sup> CD103<sup>+</sup>, CD69<sup>+</sup> CD103<sup>-</sup> and CD69<sup>-</sup> CD103<sup>-</sup> gBT-I cells were sorted from DNFB-treated skin ('Control skin') or tumour samples, respectively, and expression of the indicated genes was analysed using qPCR. Gene

expression is normalized to expression of the housekeeping genes *Hprt*, *Gapdh* and *Tbp* and shown as fold change relative to expression in CD69<sup>-</sup> populations of gBT-I cells in the spleen. **d**, WT mice were transferred naive gBT-I.CD45.1 cells and e.c. inoculated with B16.gB cells. Shown is surface expression of PD-1 by gBT-I cells isolated from the indicated organs compared with PD-1 expression in bulk CD8<sup>+</sup> V $\alpha$ 2<sup>+</sup> T cells from the same tissue at more than 3 weeks post-inoculation. **e**, Mice were transferred naive gBT-I.CD45.1 cells and e.c. inoculated with B16.gB.*Tyr*<sup>-/-</sup>.mCherry cells. Shown is the proportion of gBT-I T<sub>RM</sub> cells in peritumoural or tumour-free (non-developer) skin expressing PD-1 at more than 2–3 weeks post-inoculation. Data pooled from  $n = 4$  biologically independent experiments with  $n = 9$  (HSV, Ova),  $n = 17$  (melanoma, Ova),  $n = 5$  (non-developer, Ova),  $n = 11$  (HSV, gB),  $n = 19$  (melanoma, gB) or  $n = 9$  (non-developer, gB) mice (**a**, **b**);  $n = 2$  biologically independent experiments with  $n = 20$  (control) and  $n = 43$  (melanoma) mice per group (**c**); are representative of  $n = 2$  biologically independent experiments with  $n = 10$  mice (**d**); or pooled from  $n = 2$  biologically independent experiments with  $n = 27$  (melanoma, peritumoural) or  $n = 20$  (non-developer) mice (**e**).

## Reporting Summary

Nature Research wishes to improve the reproducibility of the work that we publish. This form provides structure for consistency and transparency in reporting. For further information on Nature Research policies, see [Authors & Referees](#) and the [Editorial Policy Checklist](#).

### Statistical parameters

When statistical analyses are reported, confirm that the following items are present in the relevant location (e.g. figure legend, table legend, main text, or Methods section).

n/a Confirmed

- The exact sample size ( $n$ ) for each experimental group/condition, given as a discrete number and unit of measurement
- An indication of whether measurements were taken from distinct samples or whether the same sample was measured repeatedly
- The statistical test(s) used AND whether they are one- or two-sided  
*Only common tests should be described solely by name; describe more complex techniques in the Methods section.*
- A description of all covariates tested
- A description of any assumptions or corrections, such as tests of normality and adjustment for multiple comparisons
- A full description of the statistics including central tendency (e.g. means) or other basic estimates (e.g. regression coefficient) AND variation (e.g. standard deviation) or associated estimates of uncertainty (e.g. confidence intervals)
- For null hypothesis testing, the test statistic (e.g.  $F$ ,  $t$ ,  $r$ ) with confidence intervals, effect sizes, degrees of freedom and  $P$  value noted  
*Give  $P$  values as exact values whenever suitable.*
- For Bayesian analysis, information on the choice of priors and Markov chain Monte Carlo settings
- For hierarchical and complex designs, identification of the appropriate level for tests and full reporting of outcomes
- Estimates of effect sizes (e.g. Cohen's  $d$ , Pearson's  $r$ ), indicating how they were calculated
- Clearly defined error bars  
*State explicitly what error bars represent (e.g. SD, SE, CI)*

*Our web collection on [statistics for biologists](#) may be useful.*

### Software and code

Policy information about [availability of computer code](#)

Data collection FACS Diva, Olympus Fluoview, BioRad ddPCR System and C1000 Touch thermal cycler, Vectra 3.3, inForm 2.3.0

Data analysis Graphpad Prism 6 and 7, Imaris 8 or 9, Adobe After Effects 11, Flowjo 9, QuantaSoft V1.7, Living Image v4.4

For manuscripts utilizing custom algorithms or software that are central to the research but not yet described in published literature, software must be made available to editors/reviewers upon request. We strongly encourage code deposition in a community repository (e.g. GitHub). See the Nature Research [guidelines for submitting code & software](#) for further information.

### Data

Policy information about [availability of data](#)

All manuscripts must include a [data availability statement](#). This statement should provide the following information, where applicable:

- Accession codes, unique identifiers, or web links for publicly available datasets
- A list of figures that have associated raw data
- A description of any restrictions on data availability

Raw data supporting the findings of this study are available from the corresponding authors upon request.

## Field-specific reporting

Please select the best fit for your research. If you are not sure, read the appropriate sections before making your selection.

Life sciences  Behavioural & social sciences  Ecological, evolutionary & environmental sciences

For a reference copy of the document with all sections, see [nature.com/authors/policies/ReportingSummary-flat.pdf](https://www.nature.com/authors/policies/ReportingSummary-flat.pdf)

## Life sciences study design

All studies must disclose on these points even when the disclosure is negative.

Sample size	Sample sizes were chosen based on prior research conducted in our laboratories to provide sufficient numbers of mice in each group to provide informative results and perform statistical testing, accounting for variability in possible disease outcomes using the epicutaneous melanoma model. For tumour challenge experiments, flow cytometric analysis experiments, ddPCR experiments, IVIS experiments and 2-PM experiments: sample sizes of n= 10 mice or more were pooled for each figure to account for the variance in disease outcomes in epicutaneously inoculated mice (60% anticipated developers, 40% anticipated non-developers). For sorting experiments: sample sizes of n= 15 B16.gB inoculated mice or more were chosen to allow enough cells to be isolated from tumours and peritumoural skins (~200/mouse) for subsequent PCR analysis.
Data exclusions	No data was excluded from analysis.
Replication	Experiments were reliably reproduced and the number of experiments performed stated in methods and legends. Culminated and pooled data is shown where possible. Where representative data is shown, relevant experiments were repeated successfully at least twice with the exact number of repeats indicated in each case. Most experiments were repeated at least twice if not 3 or more times to verify that experimental findings were reproducible. Attempts at data replication were successful within groups (i.e. developer vs. non-developer), accounting for variance in the exact proportion of mice developing (+/-60%) or not developing (+/-40%) macroscopic tumours in individual experiments.
Randomization	Animals of the same age and sex were randomly assigned to experimental groups.
Blinding	Blinding was not performed in this study. The experimental observations presented (presence or absence of a macroscopic tumour) would be consistent irrespective of blinding and therefore blinding was not relevant in this study.

## Reporting for specific materials, systems and methods

### Materials & experimental systems

n/a	Involvement in the study
<input checked="" type="checkbox"/>	<input type="checkbox"/> Unique biological materials
<input type="checkbox"/>	<input checked="" type="checkbox"/> Antibodies
<input type="checkbox"/>	<input checked="" type="checkbox"/> Eukaryotic cell lines
<input checked="" type="checkbox"/>	<input type="checkbox"/> Palaeontology
<input type="checkbox"/>	<input checked="" type="checkbox"/> Animals and other organisms
<input type="checkbox"/>	<input checked="" type="checkbox"/> Human research participants

### Methods

n/a	Involvement in the study
<input checked="" type="checkbox"/>	<input type="checkbox"/> ChIP-seq
<input type="checkbox"/>	<input checked="" type="checkbox"/> Flow cytometry
<input checked="" type="checkbox"/>	<input type="checkbox"/> MRI-based neuroimaging

## Antibodies

### Antibodies used

Antibodies used are described below:

MOUSE

Antibody, Supplier, Clone, Colour (Catalogue #) Dilution

Anti-mouse CD45.1, BD Biosciences, A20, FITC (550802); APC (561873); APCR-700 (561235); 1/200  
Anti-mouse CD45.1, eBioscience, A20, PeCy7 (25-0453-82); APC-eFluor 780 (47-0453-82); 1/200

Anti-mouse CD45.2, BD Biosciences, 104, AF700 (560693); BUV737 (564880); BV786 (563686); 1/200  
Anti-mouse CD45.2, eBioscience, 104, APC-eFluor 780 (47-0454-82); 1/100  
Anti-mouse CD45.2, Biolegend, 104, BV785 (109839)

Anti-mouse CD8a, BD Biosciences, 53-6.7, APC (561093); BUV395 (563786); BUV805 (564920); FITC (553031); 1/200

Anti-mouse CD8a, eBioscience, 53-6.7, AF700 (56-0081-82); APC-eFluor 780 (47-0081-82); 1/200 Anti-mouse CD8a, Biolegend, 53-6.7, BV605 (100743); BV711 (100747); BV785 (100749); 1/200
Anti-mouse Va2, BD Biosciences, B20.1, BV421 (566241); PE (561078); PeCy7 (560624); AF700 (561239); 1/200
Anti-mouse CD69, BD Biosciences, H1.2F3, APC (560689), BUV737 (564684), PE (553237), 1/200 Anti-mouse CD69, Biolegend, H1.2F3, BV605 (104529), 1/200
Anti-mouse CD44, BD Biosciences, IM7, BUV395 (740215), BV510 (563114), FITC (561859), PeCy7 (561861), 1/200 Anti-mouse CD44, eBioscience, IM7, AF700 (56-0441-82), 1/100
Anti-mouse CD62L, BD Biosciences, MEL-14, BV605 (743209); 1/200 Anti-mouse CD62L, eBioscience, MEL-14, PerCP Cy5.5 (45-0621-82); 1/200
Anti-mouse PD-1, BD Biosciences, J43, PE (551892); 1/200 Anti-mouse PD-1, eBioscience, J43 (25-9985-82), PeCy7; 1/200 Anti-mouse PD-1, Biolegend, PeCy7 (135216), PE (135206) 29F.1A12; 1/200
Anti-mouse IFN $\gamma$ , BD Biosciences, XMG1.2, FITC (562019), PE (562020), PeCy7 (557649); 1/100
Anti-mouse TNF, BD Biosciences, MP6-XT22, APC (561062), APC Cy7 (560658); 1/100
Anti-mouse CD103, eBioscience, 2E7, APC (17-1031-82), FITC (HMCD10301); 1/200 Anti-mouse CD103, Biolegend, 2E7, PerCP Cy5.5 (121416); 1/200
Anti-mouse KLRG1, eBioscience, FITC (11-5893-82), APC (17-5893-82), 2F1; 1/200 Anti-mouse/human KLRG1, Biolegend, MAFA, BV711 (138427); 1/200
Anti-mouse Thy1.1, eBioscience, HIS57, purified (17-0900-82) Anti-rat/mouse CD90.1 (Thy1.1), Biolegend, OX-7, AF700 (202520); 1/2500 (blood) and 1/3000 (spleen, LN, skin)
Anti-mouse CD16/CD32, BD Biosciences, 2.4G2, Purified (553142), 1/200
HUMAN
Anti-human CD8, Abcam, Ab4055, Purified, 1/800 Anti-human CD103, Abcam, Ab129202, Purified, 1/3000 Anti-human SOX10, Biocare Medical, BC34, Purified, 1/800

## Validation

All antibodies were obtained from commercial vendors and we based specificity on descriptions and information provided in corresponding Data Sheets available and provided by the Manufacturers.

## Eukaryotic cell lines

### Policy information about [cell lines](#)

Cell line source(s)	Vero cells (CSL, Australia) were used to grow HSV viruses. B16 melanoma cells were generated by the laboratory of Dr Jason Waithman (corresponding author) or laboratories of Michel Holzelt and Thomas Tuting (authors) and originally obtained from the ATCC.
Authentication	Vero cells and B16 cells were originally obtained from commercial sources (CSL or ATCC respectively) and were therefore authenticated by the manufacturer. B16 cells are true melanoma cells as they form distinctive melanoma tumours following injection to mice. Expression of relevant antigens (gB or Ova) by B16 melanoma cells has been confirmed using in vitro activation assays with transgenic T cells (gBT-I or OT-I respectively).
Mycoplasma contamination	Cell lines tested negative for mycoplasma contamination.
Commonly misidentified lines (See <a href="#">ICLAC</a> register)	No commonly misidentified cell lines were used in this study.

## Animals and other organisms

### Policy information about [studies involving animals](#); [ARRIVE guidelines](#) recommended for reporting animal research

Laboratory animals	Laboratory mouse ( <i>Mus musculus</i> ) strains C57BL/6, gBT-I, gBT-I $\times$ B6.SJL-PtprcaPep3b/BoyJ (gBT-I.CD45.1), gBT-I.Thy1.1, gBT-I.uGFP, OT-I $\times$ B6.SJL-PtprcaPep3b/BoyJ (OT-I.CD45.1), Rag1 $^{-/-}$ , Rag2 $^{-/-}$ $\times$ Il2rg $^{-/-}$ , Il15 $^{-/-}$ , Itgae $^{-/-}$ , Cd69 $^{-/-}$ , Perf1 $^{-/-}$ , Ifng $^{-/-}$ , Tnfa $^{-/-}$ , gBT-I.CD45.1 $\times$ Cd69 $^{-/-}$ , gBT-I.CD45.1 $\times$ Tnfa $^{-/-}$ and B6(Cg)-Tyr-2/J (B6 Albino) mice were bred in the Department of Microbiology and Immunology, The University of Melbourne. All transgenic strains were maintained on a C57BL/6 background. All mice were female and aged between 6 and 12 weeks of age at the time experiments commenced.
Wild animals	No wild animals were used in the study.
Field-collected samples	No field collected samples were included in the study.

## Human research participants

Policy information about [studies involving human research participants](#)

Population characteristics	All melanoma samples analyzed were from lymph node (n = 68) or skin (n = 3) metastases. Patients were selected based on clinical and pathological confirmation of cutaneous melanoma (mucosal and acral melanomas excluded) and all patients had not received any systemic treatment or radiotherapy in the biopsied area prior to surgery. A detailed clinical overview of all the patients has been previously described in Edwards J et al. Clin Cancer Res 2018, 24(13):3036-3045 (Ref. 17). Images displayed in Fig. 2 were taken from two representative patient samples with the following characteristics: (1) age: 56, gender: male, site: lymph node; and (2) age: 77, gender: female, site: subcutaneous skin.
Recruitment	The archival human melanoma samples analysed were obtained from The Melanoma Institute Australia biospecimen bank with written informed patient consent and institutional review board approval. Patients were selected based on clinical and pathological confirmation of cutaneous melanoma (mucosal and acral melanomas excluded) and all patients had not received any systemic treatment or radiotherapy in the biopsied area prior to surgery. Only archival material was analysed, no patients were recruited specifically for the current study.

## Flow Cytometry

### Plots

Confirm that:

- The axis labels state the marker and fluorochrome used (e.g. CD4-FITC).
- The axis scales are clearly visible. Include numbers along axes only for bottom left plot of group (a 'group' is an analysis of identical markers).
- All plots are contour plots with outliers or pseudocolor plots.
- A numerical value for number of cells or percentage (with statistics) is provided.

### Methodology

Sample preparation	Sample preparation is described in the Materials & Methods section.
Instrument	BD Fortessa II
Software	BD FACS Diva for collection and Flowjo 9 (Trestar) for analysis.
Cell population abundance	No cell sorting was performed in this study.
Gating strategy	<p>For spleen and LN samples, gBT-I cells were identified using the following gating strategy: FSCH lo/SSCH intermediate (lymphocytes) --&gt; FSA/FSWlo (singlet gate) --&gt; SSA/SSWlo (singlet gate #2) --&gt; Live cells (negative for PI or LiveDead differentiator) --&gt; +/- CD45.2+ (lymphocytes) where congenic marker expressed --&gt; CD8+ (CD8+ T cells) --&gt; Va2+ CD45.1+ or Va2+ Thy1.1+ (transgenic gBT-I)</p> <p>For skin and tumour samples, gBT-I cells were identified using the following gating strategy: FSCH lo/SSCH intermediate (lymphocytes) --&gt; FSA/FSWlo (singlet gate) --&gt; SSA/SSWlo (singlet gate #2) --&gt; Live cells (negative for PI or LiveDead differentiator) --&gt; +/- CD45.2+ (lymphocytes) where congenic marker expressed --&gt; +/- CD3 intermediate (T cells) --&gt; Va2+ CD45.1+ or Va2+ Thy1.1+ (transgenic gBT-I) --&gt; CD103+CD69+ (skin TRM cells)</p>

- Tick this box to confirm that a figure exemplifying the gating strategy is provided in the Supplementary Information.